Design and Application of a Proxy System Model for the Quantitative Reconstruction of Hydroclimate Variability Recorded by Oxygen Isotopes in Lacustrine Carbonate Sediment

A Thesis

SUBMITTED TO THE FACULTY OF THE

UNIVERSITY OF MINNESOTA

BY

Alejandro Fernandez

IN PARTIAL FULFILLMENT OF THE REQUIREMENTS

FOR THE DEGREE OF

MASTER OF SCIENCE

Dr. Byron Steinman

January 2021

Abstract

Oxygen isotope analyses of lacustrine sediment, which are widely used as proxies of past climatic variability, have become increasingly reliant on computational modeling approaches that allow for quantitative interpretations of past hydroclimate, constraining of water resources' sensitivities to changes in climate, and direct comparisons of proxy data with climate models. In this study, we present the development, structure and application of a Proxy System Model (PSM) designed for Castor Lake (Washington, U.S.A): a well-understood, highly monitored small lake system. The principal goal is to improve upon the understanding of the relationships between climate and the stable oxygen isotope (^{18}O) proxy system in the context of lake sediments, by addressing the impacts that a variety of climate variables, as well as non-climate relate factors such as basin morphology, vegetation, hydrological setting and lake mixing, have on the isotopic signatures of resulting sediments in the lake, as well as to provide a quantitative basis from which well-informed reconstructions of past climate can be made. Following a calibration process based on over a century of compiled daily weather data as well as approximately 14 years of in-situ continuous measurements of lake level, temperature and water oxygen isotope samples, the PSM was shown to accurately reproduce seasonal, interannual and century-scale trends of sediment oxygen isotope values and water balance, with varying degrees of accuracy for different timescales. Model-based reconstructions of hydroclimate variables for an early Holocene (~10000 years B.P.) $\delta^{18}O$ maximum in the Castor Lake sediment record show that cold-season (i.e. winter) precipitation and relative humidity must have been lower by 21% ± 5% and 14% ± 7%,

respectively, in order for the observed sediment $\delta^{18}O$ signature to be produced and recorded. Furthermore, air temperature and warm-season precipitations seem to be negligible controls on sediment $\delta^{18}O$ signatures, opposite to what was expected following the temperature dependence of carbonate sediment formation and isotopic fractionation. These results showcase the advantages of the application of PSMs to the analysis of paleoclimate proxy records as a way to make well-informed quantitative interpretations of past climate change through the constraining of physical, chemical and biological processes that impact the formation of the sedimentary archive.

Table of Contents

List of Tables

List of Figures

1. Introduction

As a result of a growing human population and climate change, water resource availability is becoming increasingly tenuous, with projections suggesting substantial reductions in effective moisture by the end of the 21st century (Dai, 2013; Schewe et al., 2014; Vorosmarty, 2000). A better understanding of how local-to-regional-scale continental hydrologic systems (drainage networks, rivers, lakes, etc.) respond to climate variability is therefore of considerable importance, especially in regions of the world where fresh water is a limiting or scarce resource due to climatic conditions, infrastructure or overexploitation. The reconstruction of past climatic conditions in these drought-sensitive regions is essential for understanding the full potential range of responses of local hydrologic systems to climate change, because evidence of past conditions of higher temperatures and lower precipitation / evaporation balances can provide insight as to what future climate contexts might hold for water resources (Mote and Salathé, 2010), especially when these reconstructions span a wide variety of time scales (multi-decadal to millennial) providing a wide spectrum of potential climate variability. In this way, water management policies can be adopted that take into account how the hydrology of a region will respond to a changing climate.

Paleoclimate reconstructions from lake sediment records provide critical insight on the dynamics and evolution of the climate system due to their widespread geographic distribution and temporal resolutions (from annual to millennial; e.g., Mann et al., 2008; PAGES2k Consortium, 2017), range of available proxies that allow for robust

interpretations (e.g., Abbott et al., 2003; Michelutti et al., 2007; Yu, 2000), and timeframes that can span thousands to millions of years (e.g., Grosjean et al., 2003; Johnson et al., 2016; Tierney et al., 2013; Williams, 1997). Additionally, the ever-growing body of paleoclimatic data from these and other types of archives, such as ice cores, corals, speleothems and marine sediments, serve as targets for the validation of model simulations of climate system dynamics (Dee et al., 2018; Hargreaves and Annan, 2009; Otto-Bliesner et al., 2014). They also allow for the constraining of the climate system's responses to both external forcing and intrinsic (i.e. random) variability on timescales which are longer than those captured by the instrumental record (Ammann et al., 2007; Mann et al., 2020; Neukom et al., 2014).

Oxygen stable isotope (^{18}O) records lacustrine sedimentary deposits containing an abundance of authigenic carbonates provide information on past changes in water isotope values (Edwards et al., 2004; Solotchina et al., 2014; Stansell et al., 2020; Steinman et al., 2019), which, depending on the lake hydrologic configuration (i.e. hydrologically closed lakes), are sensitive to changes in precipitation/evaporation balance in the catchment and the corresponding effects on lake level (Kirby et al., 2013; Shuman et al., 2010; Steinman et al., 2012). However, it has been increasingly realized that the high complexity of the lake sediment $\delta^{18}O$ proxy records, due to their non-linear relationship with any one climate variable (such as temperature or precipitation) along with other proxy- or site hydrology-specific complicating factors, makes their interpretation difficult, such that a simplified (e.g. transfer function type) approach cannot usually be applied to quantitatively or semi-quantitatively interpret these records (Gibson et al., 2016; Jones et

al., 2005; Steinman et al., 2010a). Additionally, the hydrologic context of a particular lake system can be markedly dynamic depending on the temporal variations of a number of factors such as its relation to regional or local groundwater systems, hydraulic conductivity of the catchment and lakebed sediments, extent and type of vegetation cover in its catchment, and precipitation amounts and seasonality. Due to these complications, the hydrology of a lake cannot be assumed to be constant in time, further convoluting the interpretation of ^{18}O records which relies on a proper understanding of the hydrologic context in which the authigenic sediments were formed and deposited. Computational modeling of proxy systems can be a way to assess some of these complicating factors in order to make informed interpretations of past climate changes.

Numerical models (specifically hydrologic and isotope mass-balance models) have been identified as a way to quantitatively interpret lake sediment oxygen isotope records in order to reconstruct past climate conditions (Cumming and Smol, 1993; Gibson, 2002; Gibson et al., 2016; Hostetler and Benson, 1994; Shanahan et al., 2007; Steinman et al., 2010a, 2012), through the assessment of the lake and proxy sensitivity to a variety of climate variables as well as lake-specific physical, chemical and biological processes. Furthermore, so-called Proxy System Models (PSMs) take this a step forward by aiding in the translation and comparison between climate models and climate information imbedded in proxy archives (Dee et al., 2018, 2017, 2016; Evans et al., 2013; Morrill et al., 2019) by employing a forward modeling methodology that quantifies the responses of a sensor to environmental forcing, evaluates processes by which it is placed into an archive, and assesses uncertainties that might be involved in its measurement

(Evans et al., 2013). By utilizing these computational approaches, a specific lake and a corresponding proxy system can be modeled in order to better understand its sensitivity to changes in climate, as well as to make informed and improved reconstructions of climate variables at key moments in its geologic history (e.g. when one or several climate variables such as precipitation or temperature reached a certain maximum or minimum).

As an added value, the modeling of hydrologic mass-balance within lake PSMs allows them to be used to predict water resource responses to future climate change (Kumambala and Ervine, 2010; Mbanguka et al., 2016; Yao et al., 2009). By determining water balance throughout model simulations, these predictions can be utilized in regional hydrologic models in order to better understand the specific changes in water availability that could occur under future climate scenarios in which severe drought, higher temperatures and more focalized precipitation events will likely become more common. On a more local scale, sensitivity tests and analyses can be performed in order to quantify lake vulnerability to specific changes in regional climate and therefore to develop sound preservation and management strategies, especially for communities that might heavily depend on lake systems as water sources for their sustenance and agriculture (Lempert and Groves, 2010).

Here, we showcase the structure and application of a PSM of the lacustrine carbonate sediment $\delta^{18}O$ proxy applied to Castor Lake: a small, closed-basin lake in the Upper Columbia River basin of Northcentral Washington State, U.S.A., wherein lake levels and meteorological data have been continuously recorded on site for a period of approximately 14 years. The PSM presented here is based on the model of Steinman et al.

(2010a, 2013) with several important modifications. The main objectives of this research are to: 1. Present the design and implementation methodology of a PSM to a specific proxy system; 2. Test the applicability of the PSM to accurately predict changes in lake level and isotopic composition of the carbonate sediment that makes up the lake sedimentary record; 3. Produce a quantitative reconstruction of climate variables in the early Holocene time period, approximately 10000 years BP (which through multiple lines of evidence is known to have been significantly drier than present) as an example of the applicability of the proposed methodology; and 4. Assess the possible sources of uncertainty and error that might be affecting the interpretations of this, and similar proxy records.

2. Background

2.1. Oxygen Stable Isotope Proxy

Stable Oxygen isotope measurements (i.e. ^{18}O) can be utilized as tracers of moisture source and transport through the hydrologic cycle as the heavy isotopologues of water with respect to Oxygen are stable and fractionation is well understood (Bowen and Revenaugh, 2003). As water vapor – sourced from the tropical oceans – makes its way into the continental interiors in the high latitudes by atmospheric transport, it experiences isotopic depletion in the form of Rayleigh distillation (Rozanski et al., 1992) along a predictable trend known as the Global Meteoric Water Line (GMWL). This is due to the continuous decrease in temperature of air masses as they travel inland, leading to condensation and precipitation, during which the heavier isotopologues of water are

preferentially incorporated into the liquid or solid forms of water. Similarly, this temperature-dependent process leads to an isotopic enrichment of warm-season precipitation over cold-season precipitation in the high latitudes. Local and regional trends in water isotopic compositions are therefore highly seasonal in fluvial and lacustrine water bodies, as their compositions are primordially controlled by precipitation or snowmelt. However, secondary fractionation processes can further modify the ^{18}O composition of water molecules in surficial water bodies throughout their residence time in the continents.

In closed-basin lake systems, evaporation is considered to be a major control in the lake's water budget, leading to increased fractionation of water in terms of its ^{18}O isotopic composition (Lloyd, 1966). This is because as water evaporates from the lake surface, especially during dry and warm summers, the lighter isotopes are preferentially mobilized through kinetic fractionation processes to the escaping vapor, leaving behind isotopically heavier water molecules (Gat, 1996). Thus, although baseline isotopic composition values for lake systems are controlled by precipitation alone, closed lakes experience further fractionation and their isotopic signatures plot on a different trend than meteoric water known as the Local Evaporative Line (LEL). These differences in isotopic composition can be utilized in order to quantify the extent of evaporative control on a lake's hydrologic budget (Li and Ku, 1997). As such, the isotopic composition of lake water in these systems is reflective of precipitation vs. evaporation balances, with more positive (negative) values occurring during drier (wetter) conditions, and it is therefore indicative of regional climate, rather than exclusively of the original isotopic

compositions of meteoric water. Authigenic carbonate sediments, when they're formed in isotopic equilibrium with the water column, can record the isotopic composition of the water at the time of formation (*see equations 31-32)*, with a secondary water-temperature effect (Kim and O'Neil, 1997).

Oxygen stable isotope records have been utilized extensively in the literature in order to better understand past climate variability in a variety of timescales and geographic locations (Holmes et al., 2007; Seal and Shanks, 1998; Stansell et al., 2013; Steinman et al., 2012). As records of precipitation vs. evaporation balance, they can give valuable insight into the variability of moisture availability in a variety of timescales, which can be utilized in order to better understand the extent of climate variability in a specific region. In order to properly interpret and understand ^{18}O records from the sedimentary archives or closed-basin lakes, however, it is paramount to constrain the wider range of factors that might influence water – and therefore sediment – isotopic compositions, such as moisture source variability and seasonality, hydrology of the basin, biological activity in the water column, (Edwards et al., 2004; Gonfiantini, 1986; Henderson and Shuman, 2009; Jones et al., 2005; Steinman et al., 2010a, 2010a) among others. In order to constrain these factors and aid in the determination of climatic signals from heavy Oxygen isotope records from lacustrine sediments, computational models that take into account physical, chemical and biological variability intrinsic to individual lakes are considerably useful and have become necessary tools to produce paleoclimate records.

2.2. Proxy System Modeling

Isotope mass-balance models can provide a quantitative constraining of several non-climatic processes that may influence the isotopic composition of lake water in individual systems (Hostetler and Benson, 1994; Jones and Imbers, 2010; Shapley et al., 2008; Steinman et al., 2010a, 2010a). Thus, their application has become increasingly more commonplace in paleoclimate studies in order to produce well-informed, quantitative paleoclimatic reconstructions (Cumming and Smol, 1993; Gibson, 2002; Hostetler and Benson, 1994; Steinman et al., 2013, 2013) and to utilize these paleo data for the calibration or testing of climate models (Dee et al., 2018, 2017, 2016; Evans et al., 2013; Morrill et al., 2019; Otto-Bliesner et al., 2014). Utilizing hydrologic and isotope mass balance calculations (*see equations* 1 *and* 2), together with site-specific observational data – such as lake levels, inflows and outflows, and water isotopic compositions – theoretical frameworks of the fundamental dynamics of isotopic fractionation and mixing can be added into interpretations of ^{18}O records (e.g., Dinçer, 1968; Gat, 1996; Gonfiantini, 1986), allowing for the quantitative assessment of the climatic context in which a specific isotopic composition value may be produced. Therefore, computational models of specific lake systems can give insights as to what are the most influential factors on proxy values, both climate and non-climate related, and can inform reconstructions emphasizing these factors (Steinman et al., 2013).

In a review, Evans et al. (2013) describe Proxy System Models (PSM) as a forward modeling basis for the interpretation and comparison of proxy data; and they identify four distinct submodels that comprise a theoretical PSM: *Environment, Sensor,*

Archive and *Observation* (an *Archive* is the medium in which the responses of a *Sensor* to *Environmental* forcing is recorded; Evans et al., 2013; Figure 2). Specifically, for the model presented here, the *Environment* submodel corresponds to all the factors that are considered to control or influence the isotopic composition of the lake water (i.e., climate variables and hydrologic balance). This submodel corresponds mostly to the hydrologic and isotope mass-balance model first presented by Steinman et al. (2010a, 2010a) which takes climatic inputs and hydrologic parametrizations (*see* Environment Submodel) to simulate a water balance (i.e., lake level) and isotopic composition response. These two variables are the outputs from the *Environment* submodel and are input into the *Sensor* submodel which in essence simulates the formation of authigenic sediment in the water column and the simultaneous isotopic fractionation processes that result in a modeled isotopic composition of sediment. The *Archive* submodel compiles simulated sediment isotopic compositions into records that can be utilized as the basis for comparison with actual proxy datasets from the lake's sedimentary archives. Finally, the *Observation* submodel aims to take into account the uncertainties related to the development of proxy data from sediment cores, such as age-model and analytical uncertainties, and couple them to the simulated or modeled records from the *Archive* submodel.

3. Study area

The development and calibration/validation of the PSM presented in this study was based on, and applied to, the hydrologic and sedimentary system of Castor Lake, due to the considerable understanding and available literature on this system's hydrology and

water-isotope dynamics that govern the oxygen stable isotope sedimentary proxy archive (i.e., *Sensor* and *Archive* conceptual models; Nelson et al., 2011; Steinman et al., 2019, 2013, 2010b, 2010a). Castor Lake (48.54˚ N, 119.56 ˚ W; 601 masl) is a small (~0.06km^2), closed-basin kettle lake in the Eastern Cascade Range of the North American Pacific Northwest (Figure 1), characterized by relatively high alkalinity (450-575 mg/L as $CaCO_3$; Steinman et al., 2019) and salinity (>2000 mg/L; Nelson et al., 2011). The water residence time has been estimated by previous modeling studies (Steinman et al., 2010a) as approximately 2.5 years, and surficial water samples plot on the Local Evaporative Line (Steinman et al., 2013), indicating that evaporation is the major water-loss pathway – hence its high salinity – although considerable groundwater infiltration and outseepage also influence its water balance. The catchment area (~0.86 km^2) is vegetated mostly by shrub-steppe, evergreen and secondary deciduous vegetation and is located on an elevated terrace margin of the Okanogan River, which isolates the lake from regional groundwater, limiting the water inputs to precipitation and shallow groundwater influx from the immediate catchment. Bedrock geology in the surrounding Lime Belt region is dominated by calcareous sedimentary and metamorphic rocks, as well as some basalt flows (Rinehart and Fox, 1976).

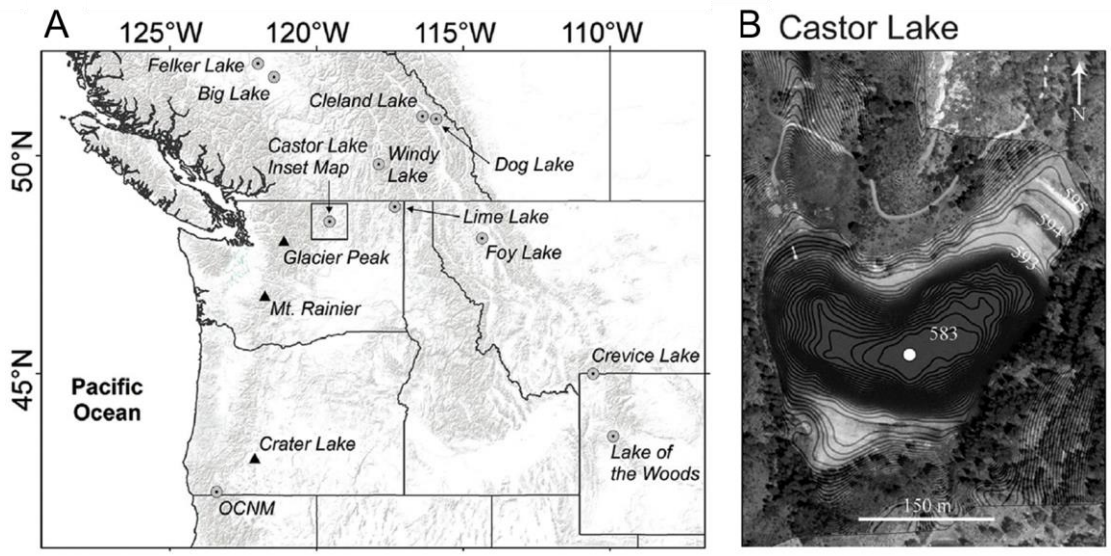

Figure 1. **A:** Map of the Pacific Northwest region of North America, showing the location of several continental paleoclimate records, including Castor Lake. **B:** Bathymetric map of the Castor Lake catchment. White dot indicates coring location. Modified from Steinman et al., (2019).

Seasonal water column profiles (Steinman et al., 2019) indicate a monomictic stratification regime that leads to a warm, saline epilimnion during the spring, summer and early fall and mixing during fall as a result of the breakdown of thermal stratification. These conditions in the epilimnion promote the formation of authigenic carbonate sediment as surface waters experience a temperature increase, lowering the solubility of $CaCO_3$ as well as increasing the concentration of Ca^{2+} and HCO_3^{2-}/CO_3^{2-} ions (Steinman et al., 2013), and facilitating the formation of carbonate mineral crystals (in the form of aragonite) that make-up the Holocene sedimentary record at Castor Lake (Nelson et al., 2011). However, the formation of aragonite early in the stratified season depletes the water of Ca^{2+} ions, making the formation of carbonate sediment in the lake Calcium-limited. Thus, catchment groundwater influxes during the spring and summer with

dissolved Ca^{2+} - sourced from the catchment's predominant carbonate bedrock – are a controlling factor on the extent of authigenic aragonite formation through the warm season.

4. Methods

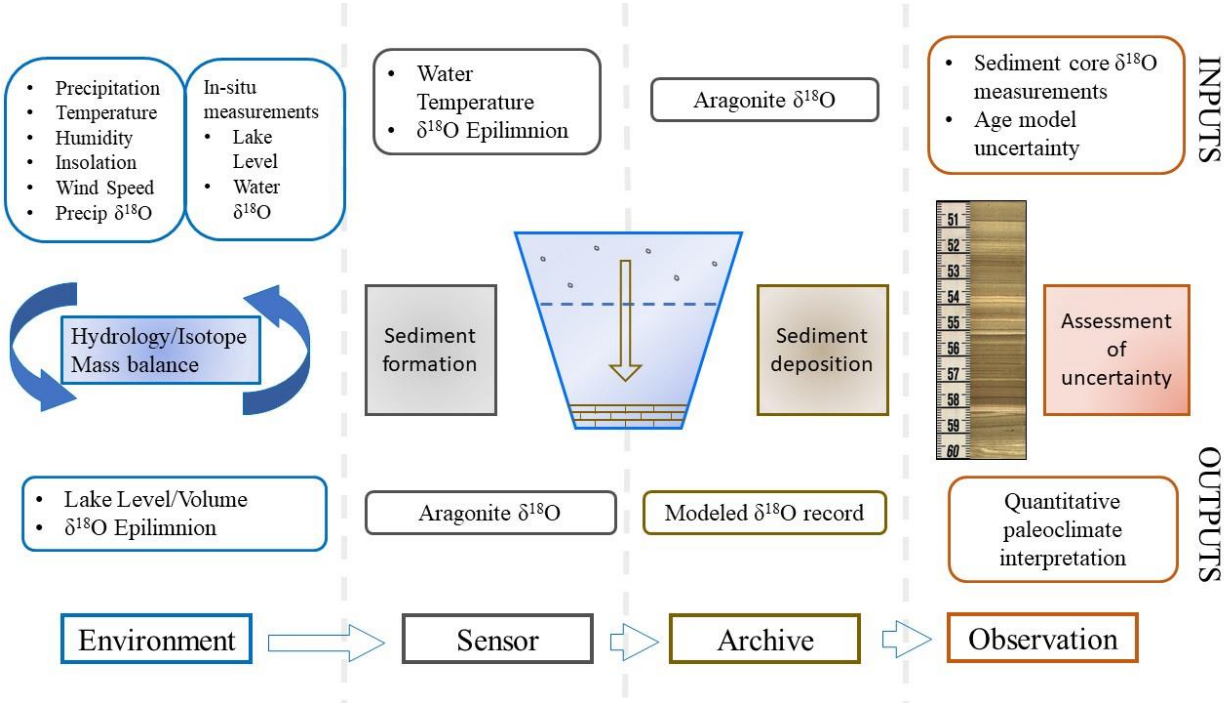

Figure 2. Schematic of the four submodels that make up this study's PSM – as conceptualized by Evans et al. (2013). The conceptual flow is summarized from left to right, as the model starts with the Environment submodel in order to produce the Observation submodel outputs. The input data for each submodel is shown towards the top of the schematic, and the outputs towards the bottom.

The PSM presented in this paper follows the conceptual forward modeling methodology described by Evans et al. (2013), in which the model predicts a climate proxy value – in this case carbonate sediment $\delta^{18}O$ – from site-specific inputs, parameter values and climate variables. In the case of the Castor Lake model, the site-specific inputs

are related to catchment and basin morphology, soil moisture capacity of the soil, and lake mixing, among others (*See* **Model Inputs**). To this end, the *Environment*, *Sensor*, *Archive* and *Observation* subcomponents of the proxy system (Evans et al., 2013; Dee et al., 2018) are individually assessed in order to determine to what extent the proxy values are a product of local or regional climate variability versus other site- and proxy-specific processes (Figure 2). Hence, paleoclimate scenarios can be quantitatively reconstructed based on a series of iterative calculations that transform climate inputs, hydrology, isotope geochemistry, isotopic fractionation and sediment formation into proxy values that are analyzed on relevant timescales. The model structure is based on the work of (Steinman et al., 2010a, 2010b), run in MATLAB® at a sub-daily timestep (changed from a monthly time-step from previous applications) in which the *Environment* subcomponent corresponds to the hydrologic and isotopic mass-balance calculations for the lake, the *Sensor* refers to the physicochemical processes that results in $\delta^{18}O$ signatures in endogenic carbonate sediment (including assessment of the uncertainties in timing and depth within the water column of formation), the *Archive* is the sedimentation of these carbonate minerals as well as possible re-suspension and mixing of the upper sedimentary layers, and finally the *Observation* subcomponent is mostly related to the age model uncertainties from sediment cores as well as analytical uncertainty from isotopic ratio measurements. These four subcomponents, or submodels, are described in detail below:

4.1. Environment submodel – Hydrologic and Isotope mass balance

The *Environment* submodel comprises the external climate inputs and catchment- or lake-specific variables that have a direct influence on the lake's hydrology or isotopic composition of the water. The outputs of the *Environment* submodel are the lake's resulting water balance and isotopic signatures; the latter directly controls the *Sensor* submodel as its input. Because this model is run on a daily timestep, all climate inputs correspond also to daily values (*See* **Model Inputs**). This allows for the detection and quantification of the impacts that extreme precipitation events (e.g. heavy storms) and heat waves can have on the hydrology and isotopic composition of the lake water, which are likely to considerably influence the paleoclimate sensor of the proxy system (i.e. sediment $\delta^{18}O$ signatures) and might be lost in monthly averages. The structure of the *Environment* submodel mainly consists of the mass-balance calculations (equations 1-2) and is identical to the hydrologic and isotope mass-balance model from Steinman (2010a), variations of which have been applied to a variety of paleoclimate studies (Nelson et al., 2011; Rosenmeier et al., 2016; Stansell et al., 2020, 2013; Steinman et al., 2012).

4.1.1. Mass-balance Equations

The hydrologic and isotope mass-balance of the *Environment* submodel are fundamentally described by the mass-balance equations below:

$$\frac{dV_L}{dt} = \Sigma I - \Sigma O \qquad (1)$$

$$\frac{dV_L\delta_L}{dt} = \Sigma I\delta_I - \Sigma O\delta_O \qquad (2)$$

where ΣI indicates the sum of all the hydrologic influxes and ΣO indicates the sum of all the outfluxes to and from the lake. V_L is the total lake volume at time t and δ corresponds to the isotopic composition of the specific hydrologic flux. These equations represent the hydrologic (equation 1) and isotopic (equation 2) mass balance for the lake system and are applied to each distinct water reservoir in the model. In the *Environment* submodel there is a total of six reservoirs: shallow and deep lake water reservoirs (which correspond to the epilimnion and the hypolimnion, during the stratified months), shallow and deep soil water, snowpack, and runoff/groundwater. This latter reservoir is not an actual real-world reservoir, but rather is a conceptual construct that allows for the representation of the transit time of runoff or shallow groundwater fluxes through the catchment.

Table 1. Conventions and abbreviations of model variables.

Abbreviation	Name	Units	Abbreviation	Name	Units
a , b	Exponential Outseepage Parameters (Model Parameters)		F_{SSI}	Shallow Soil Infiltration (From Catchment) Flux	m^3/day
a_u	Penman Wind Function Constant	-	h_n	Temperature-Normalized Relative Humidity	%
ALB_C	Catchment Albedo	-	OS	Outseepage flux	cm/day
ALB_W	Water Surface Albedo	-	OS	Outseepage per unit area	m/day
AWC_{DS}	Available Water Capacity - Deep Soil Reservoir	cm	PET	Potential Evapotranspiration per unit area	m/day
AWC_{SS}	Available Water Capacity - Shallow Soil Reservoir	cm	Ra	Daily Extraterrestrial Radiation	MJ/m2/day
C	Experimentally Derived Isotopic Separation Value	‰	RES_{DL}	Deep Lake Reservoir	m^3
C_{IN}	Inflow Delay Constant (Model Parameter)	-	RES_{DS}	Deep Soil Reservoir	m^3
CA	Catchment Area	km2	RES_{IN}	“IN” Reservoir	m^3
E	Evaporation per unit area	mm/day	RES_{SL}	Shallow Lake Reservoir	m^3
e_{s-a}	Air Vapor Pressure	mbar	RES_{SP}	Snowpack Reservoir	m^3
e_{s-w}	Water Vapor Pressure	mbar	RES_{SS}	Shallow Soil Reservoir	m^3
F_{DLM}	Deep Lake Mixing Flux (to Shallow Lake Reservoir)	m^3/day	RH	Relative Humidity	RH
F_{DOS}	Deep Outseepage Flux (from Deep Lake Reservoir)	m^3/day	Rs	Incoming Solar Radiation	MJ/m2/day
F_{DSD}	Deep Soil Drainage Flux (to “IN” Reservoir)	m^3/day	SVC	Shallow Lake Volume Control	m3

F_{DSE}	Deep Soil Evapotranspiration	m^3/day	T_w	Shallow Lake Water Temperature	˚C
F_E	Evaporation from Lake Surface Flux	m^3/day	Ta	Air temperature	˚C
F_{IN}	"IN" Reservoir Flux to Lake	m^3/day	WS	Wind Speed	m/s
F_{OF}	Lake Surficial Overflow Flux	m^3/day	α	Equilibrium Fractionation Factor	-
F_P	Direct Precipitation on Lake Surface Flux	m^3/day	δ	Isotopic composition of the specified flux or reservoir	‰
F_{RO}	Catchment Runoff Flux	m^3/day	δ_A	Atmospheric Isotopic Composition	‰
F_{SF}	Snowfall on Catchment Flux	m^3/day	δ_{arag}	Isotopic Composition of Authigenic Aragonite	‰
F_{SLM}	Shallow Lake Mixing Flux (to Deep Lake Reservoir)	m^3/day	δ_E	Isotopic Composition of Water Vapor from Lake Surface Evaporation	‰
F_{SM}	Snowmelt Flux	m^3/day	δ_L	Isotopic Compositions of Shallow Lake Water	‰
F_{SOS}	Shallow Outseepage Flux (from Shallow Lake Reservoir)	m^3/day	ε_{eq}	Equilibrium Isotopic Separation	‰
F_{SSD}	Shallow Soil Drainage (to Deep Soil Reservoir)	m^3/day	ε_{kin}	Kinetic Isotopic Separation	‰
F_{SSE}	Shallow Soil Evapotranspiration Flux	m^3/day	ε_{tot}	Total Isotopic Separation	‰

4.1.2. Hydrologic Mass Balance

Equations (3) and (4) show how the volume of water in the lake changes over time by addition of runoff and shallow groundwater, precipitation over the lake and the subtraction of outseepage (as an exponential function of distance from shore), evaporation and overflow fluxes. Additionally, mixing fluxes for shallow and deep water (F_{SLM} and F_{DLM}) also control the water balance within the lake's water column (*See* **Seasonal Stratification**). The units of all volumetric reservoirs (RES) and fluxes (F) are [m^3] and [m^3day^{-1}], respectively. To prevent unrealistic scenarios that might come about due to calculations on empty reservoirs, all negative volumetric fluxes are adjusted to zero. The value of the timestep of model iteration *dt* was 1/8 day, by which all daily fluxes are multiplied.

$$\frac{dRES_{SL}}{dt} = F_P + F_{IN} + F_{DLM} - F_E - F_{SLM} - F_{SOS} - F_{OF} \tag{3}$$

$$\frac{dRES_{DL}}{dt} = F_{SLM} - F_{DLM} - F_{DOS} \tag{4}$$

Precipitation over the lake surface area (F_P) is determined based on the daily precipitation values from climate data, and evaporation from the lake surface is estimated by a combination radiation-aerodynamic Penman method (equation 21).

The hydrology of the soil reservoirs (RES_{SS} and RES_{DS}) is calculated by the amount of infiltration that happens throughout the catchment from rainfall and snowmelt (F_{SSI}; equation 11) as well as catchment evapotranspiration – itself divided into

evapotransipirative loss from the shallow soil (F_{SSE} ; equation 14) and from the deep soil (F_{DSE} ; equation 16) as follows:

$$\frac{dRES_{SS}}{dt} = F_{SSI} - F_{SSE} - F_{SSD} \quad (5)$$

$$\frac{dRES_{DS}}{dt} = F_{SSD} - F_{DSE} - F_{DSD} \quad (6)$$

where only the water volume leftover once both shallow and deep soil reservoirs are saturated (F_{DSD}; equation 17) recharges the Inflow Reservoir (RES_{IN}) (equation 7). The hydrologic balance of this Inflow Reservoir is modeled as:

$$\frac{dRES_{IN}}{dt} = F_{RO} - F_{DSD} - F_{IN} \quad (7)$$

where F_{RO} corresponds to the runoff flux from the catchment that happens whenever saturation of the shallow soil occurs due to precipitation (equation 12). As the "IN" reservoir fills up, it simultaneously discharges its volume following equation 13.

The balance of the Snowpack Reservoir is described as:

$$\frac{dRES_{SP}}{dt} = F_{SF} - F_{SM} \quad (8)$$

where F_{SF} is the snowfall flux which corresponds to daily precipitation amounts over the catchment whenever air temperatures fall below 0˚C, and F_{SM} is the snowmelt flux, calculated based on the model of Vassiljev et al. (1995), where melting occurs at a rate of 0.7mm $^{\circ}C^{-1}$ day^{-1}, at temperatures greater than -2˚C as:

$$F_{SM} = 0.0007 * (T_a + 2) * CA \quad (9)$$

4.1.3. Infiltration, runoff and catchment inflow

Based on the two-layer soil models of Palmer (1965) and Vassiljev et al. (1995), this system of hydrologic flux equations controls the division of available water from precipitation into soil storage, runoff and subsurface inflow to the lake. Available water capacities for the individual soil reservoirs were determined from total estimated soil water capacity (AWC; *see* **Model Inputs**) as:

$$AWC_{SS} = AWC_{DS} = AWC_{SS} * \left(\frac{1}{2}\right) * AWC_{mod} \tag{10}$$

AWC_{SS} and AWC_{DS} represent the available water capacities of the shallow and deep soil reservoirs, respectively. AWC_{mod} is a model parameter that modifies the total soil water capacity (*see* **Model Calibration)**. Infiltration into the shallow soil reservoir occurs from rainfall or snowmelt within the catchment, only when the water capacity of the reservoir has not been reached, as follows:

$$F_{SSI} = \begin{cases} F_R + F_{SM} & RES_{SS} < CA * AWC_{SS} \\ (F_R + F_{SM}) * \frac{1}{2} & RES_{SS} \geq CA * AWC_{SS} \; and \; RES_{DS} < CA * AWC_{DS} \\ 0 & RES_{SS} \geq CA * AWC_{SS} \; and \; RES_{DS} \geq CA * AWC_{DS} \end{cases} \tag{11}$$

where CA denotes the catchment area [m^2]. When the shallow soil reservoir is saturated, half of the water available for infiltration is transferred into the Deep Soil Reservoir. Once both reservoirs are full, no water is available for infiltration and all the available water is then considered runoff, following the expression:

$$F_{RO} = \begin{cases} F_R + F_{SM} & RES_{SS} \geq CA * AWC_{SS} \text{ and } RES_{DS} \geq CA * AWC_{DS} \\ (F_R + F_{SM}) * \frac{1}{2} & RES_{SS} \geq CA * AWC_{SS} \text{ and } RES_{DS} < CA * AWC_{DS} \\ 0 & RES_{SS} < CA * AWC_{SS} \end{cases} \quad (12)$$

The flux of water from the Inflow Reservoir into the lake is modeled by the equation:

$$F_{IN} = RES_{IN} * C_{IN} \quad (13)$$

where C_{IN} is a model parameter denoted here as the Inflow Delay Constant. The value for this parameter is empirically derived (*see* **Model Calibration**), and is meant to represent the lag in time, as well as any unaccounted-for volumetric losses, in runoff and shallow groundwater inputs into the lake water due to the movement of water through the porous and heterogeneous soil medium, as well as surficial travel time during precipitation events.

Equations 11 and 12 deal with all the available catchment-sourced water either as direct runoff or as infiltration into the soil reservoirs. The latter scenario, in turn, leaves water in the soil reservoirs susceptible for evapotranspiration, where it can be lost from the catchment. This evapotranspiration flux from the catchment is determined by potential evapotranspiration (PET [m/day]; equation 22) as well as the volume of water stored in the soil as:

$$F_{SSE} = \begin{cases} PET * CA & RES_{SS} > PET * CA \\ RES_{SS} & RES_{SS} \leq PET * CA \end{cases} \quad (14)$$

When the volume of water in the shallow soil reservoir is greater than the evapotranspiration flux, the remaining volume infiltrates into the Deep Soil Reservoir. This is calculated following the expression:

$$F_{SSD} = RES_{SS} - CA * AWC_{SS} \tag{15}$$

where F_{SSD} is the shallow soil drainage flux. Similarly, the Deep Soil Reservoir is also subject to evapotranspiration losses, which are calculated as a function of F_{SSE} as:

$$F_{DSE} = \begin{cases} PET * CA - F_{SSE} & RES_{DS} > CA * PET - F_{SSE} \\ RES_{DS} & RES_{DS} \leq CA * PET - F_{SSE} \end{cases} \tag{16}$$

Any volume of water left in the Deep Soil Reservoir after evapotranspiration demands and available water capacities have been met gets transferred to the Inflow Reservoir as the deep soil drainage flux (F_{DSD}):

$$F_{DSD} = RES_{DS} - CA * AWC_{DS} \tag{17}$$

4.1.4. Lake Mixing

According to field observations (Steinman et al., 2010a), the seasonal cycle of mixing of the lake water column behaves as follows: after the summer ends and evaporation rates decrease, precipitation saturates the soil and lake level begins to increase from its early fall minimum. Simultaneously, thermal stratification breaks down and the lake mixes due to the cooling of the epilimnion. With the onset of winter, ice forms on the surface and thickens throughout the cold season; simultaneously, catchment snowpack accumulates as the highest amounts of precipitation of the hydrologic year

occur during the cold season and no water flows into the lake. As temperatures warm in the spring, the melting of lake ice creates a fresh-water cap that is enhanced by the thawing of the Snowpack Reservoir which brings isotopically light, low salinity water into the lake. Due to wind action and the warming of the epilimnion, the water column is readily mixed, homogenizing isotopic composition and salinity of the lake. Lastly, once the "pulse" of meltwater and increased runoff subsides, around mid to late spring, evaporation rates begin to increase as air temperatures rise and precipitation decreases, and the surface layer of the lake begins to get isotopically enriched and the warm season water column stratification is established.

In order to quantitatively model the mixing regime, the volume of the shallow lake reservoir is independently controlled by the mixing depth (MD) variable. The monthly values for this variable were first determined by Steinman et al. (2010b) through field observations over a three-year period; these measurements showed that the epilimnion develops in April, and continues to thicken through July, when it reaches its maximum depth (~6.0m) and stays that way until November, when the lake mixes. Thus, if the shallow lake reservoir at any time has more water volume than that permitted by the Mixing Depth variable at a specific day of the year, the shallow lake mixing flux sends that excess water to the shallow lake reservoir. Similarly, during the months of winter in which shallow lake reservoir has a volume of zero, the lake is assumed to be completely mixed and therefore only one water reservoir is considered. The following equations characterize these processes:

$$F_{DLM} = \begin{cases} 0 & Nov < t \leq Dec \\ SVC - RES_{SL} & Jan < t \leq Oct \end{cases} \quad (18)$$

$$F_{SLM} = \begin{cases} 0 & Jan < t \leq Sep \\ RES_{SL} & Oct < t \leq Dec \end{cases} \quad (19)$$

where SVC is the shallow lake volume control, determined by the mixing depth measurements for each day of the year, and calculated as the volume of the shallow lake reservoir based on mixing depth and bathymetry.

4.1.5. Lake Outseepage

Lake outseepage (or infiltration) is modeled after Steinman et al. (2012) and accounts for water losses though the lake bed, wherein an exponential function is applied in which the outseepage rate – or flux – decreases as the distance from shore increases. Several studies of lakes with different hydrologic configurations have determined that outseepage through the lakebed is greater through the coarser sediments emplaced in the higher energy depositional settings of shorelines than through the fine, clay sized sediments that accumulate at greater depths farther from the shoreline (Cherkauer and Zager, 1989; Genereux and Bandopadhyay, 2001; Pfannkuch and Winter, 1984; Rautio and Korkka-Niemi, 2011; Shaw and Prepas, 1990). Nonetheless, some studies have also found lakes that do not necessarily follow this expected trend, proposing that local groundwater configurations and/or stratigraphic controls on catchment-lake bed interactions lead to unexpected scenarios where hydraulic conductivity is highest at the lake-bed center (Cherkauer and Nader, 1989; Kidmose et al., 2013; Schneider et al., 2005; Vainu et al., 2015). However, Castor Lake surficial sediment samples indicate a

fining toward the depocenter (Steinman et al., 2010a) and water $\delta^{18}O$ samples attest to high levels of freshwater inputs to the lake near the shore, thereby supporting the application of an exponential outseepage function to model how water flows out of the lake and eventually makes its way into the regional groundwater. Thus, outseepage from the lake is modeled by the expression:

$$OS = a * exp\left(-\frac{x}{b}\right) \tag{20}$$

where OS is the outseepage flux [m/day], a and b are parameters whose values are empirically derived through the model calibration process and x denotes distance from shore [m]. The model calculates a value for OS for every 20cm horizontal slice of the basin bathymetry (*see* **Model Inputs)**, as well as a value of surface area through which the outseepage will occur. Then, a volumetric flux is computed (by multiplying OS by the surficial area of the corresponding slice) and the total outseepage flux for the entire water column is then obtained by integrating over the lake depth at that specific moment in time.

4.1.6. Lake surface evaporation and catchment evapotranspiration

The evaporation and evapotranspiration calculations presented here are based on simplified version of the modified Penman equation from Valiantzas (2006). These equations were chosen based on the availability of local meteorological data, as well as the ability of the method to produce values similar to those of energy budget methods (Buso and Likens, 2007). Both are described as follows:

$$E = [0.051 * (1 - ALB_W) * R_S * (T_a + 9.5)^{\frac{1}{2}} - 2.4 * \left(\frac{R_S}{R_a}\right)^2$$

$$+ 0.052(T_a + 20) * \left(1 - \frac{RH}{100}\right) * (a_u - 0.38 + 0.54 * WS] \quad (21)$$

$$PET = [0.051 * (1 - ALB_C) * R_S * (T_a + 9.5)^{\frac{1}{2}} - 2.4 * \left(\frac{R_S}{R_a}\right)^2$$

$$+ 0.048(T_a + 20) * \left(1 - \frac{RH}{100}\right) * (0.5 + 0.536 * WS] \quad (22)$$

where E is the evaporation flux from the lake surface [mm/day] and PET is the potential evapotranspiration flux [mm/day] from the catchment soil moisture and runoff reservoirs. ALB_w is the albedo of the lake surface (0.08) and ALB_c is the average albedo value of the catchment (0.25). T_a is average daily temperature [^oC], R_s is the average daily incoming solar radiation or insolation [MJ/m^2/day], R_a is the average daily extraterrestrial radiation [MJ/m^2/day], RH is the average daily relative humidity [%], WS is the average daily windspeed [m/s] and a_u is the Penman wind function constant. It is worth noting that E and PET are set to zero whenever air temperature is below freezing.

4.1.7. Isotopic mass-balance

Isotope mass-balance is determined for each reservoir by multiplying each flux in the hydrologic model by its corresponding isotopic composition (denoted in standard δ notation as the deviation from Vienna Standard Mean Ocean Water – VSMOW). These calculations follow the equations from Dinçer (1968), Gonfiantini (1986), and Hostetler and Benson (1994).

Evaporation from the lake surface is the only isotopic fractionation process in the *Environment* model, which means it is the only flux that changes the isotopic composition of its source. More specifically, as evaporation from the lake surface becomes the main control on the lake water balance during the summer, the lighter ^{16}O isotope is preferentially removed, significantly enriching the epilimnion until precipitation amounts increase in the fall and evaporation rates decline. The isotopic fractionation of lake surface evaporation is calculated with the linear resistance model of Craig and Gordon (1965):

$$\delta_E = \frac{\alpha^* * \delta_L - h_n * \delta_A - \varepsilon_{tot}}{1 - h_n + \varepsilon_{kin} * 0.001} \tag{23}$$

where α^* is the reciprocal of the equilibrium isotopic fractionation factor, $\delta_L$is the isotopic composition of the shallow lake water, h_n is temperature-normalized relative humidity, δ_A is the atmospheric isotopic composition (assumed to be in isotopic equilibrium with precipitation $\delta_A = \delta_P - \varepsilon_{eq}$; (Gibson, 2002)), ε_{tot} is the total isotopic separation ($\varepsilon_{tot} = \varepsilon_{kin} + \varepsilon_{eq}$), and ε_{kin} and ε_{eq} correspond to the kinetic and equilibrium isotopic separations, respectively.

The equilibrium fractionation factor is a function of water temperature, and is calculated using the equations from (Horita and Wesolowski, 1994):

$$ln\,\alpha = 0.35041 * \left(\frac{10^6}{{T_w}^3}\right) - 1.6664 * \left(\frac{10^3}{{T_w}^2}\right) + 6.7123 * \left(\frac{1}{T_w}\right) - 7.685 * 10^{-3} \tag{24}$$

and

$$\alpha^* = \frac{1}{\alpha} \tag{25}$$

The per mil equilibrium isotopic separation for oxygen and hydrogen is given by the expression:

$$\varepsilon_{eq} = 1000 * (1 - \alpha^*) \tag{26}$$

The kinetic fractionation is a function of moisture deficit and molecular diffusion over the water surface and is estimated with the following expression (Merlivat and Jouzel, 1979):

$$\varepsilon_{kin} = C * (1 - h_n) \tag{27}$$

in which $1 - h_n$ represents the moisture deficit over the lake surface, and C is the experimentally derived isotopic separation value (14.3‰) (Araguás-Araguás et al., 2000; Vogt, 1976).

Normalized relative humidity corresponds to the ratio of vapor pressures of the overlying air and the surface water (both in mbar), multiplied by the relative humidity:

$$h_n = RH * \frac{e_{s-a}}{e_{s-w}} \tag{28}$$

$$e_{s-a} = 6.108\, exp\left(\frac{17.27 * T_a}{T_a + 237.7}\right) \tag{29}$$

$$e_{s-w} = 6.108\, exp\left(\frac{17.27 * T_w}{T_w + 237.7}\right) \tag{30}$$

4.2. Sensor Submodel – Sediment $\delta^{18}O$

The *Sensor* submodel turns the outputs of the *Environment* submodel (i.e. lake volume and isotopic composition of the water) into the signal that is measured as the climate proxy: in this case, the $\delta^{18}O$ signature of the authigenic carbonate sediment. In Castor Lake, which has a closed-basin configuration and is isolated from regional groundwater, this sensor is mostly sensitive to precipitation/evaporation balance changes (Steinman et al., 2010a, 2010b). However, many other factors can influence the isotopic signatures of the epilimnion water – where the endogenic sediment is formed – such as seasonal shifts in meteoric water $\delta^{18}O$ signatures, as well the timing of formation of endogenic aragonite and the timing and depth of stratification of the water column.

The input to the *Sensor* submodel is the mean value of isotopic composition of the epilimnion lake water in VSMOW notation. This value is then utilized to compute the sediment isotopic composition, which is assumed to capture the modeled value of the paleoclimate "sensor" at the moment of sediment formation in the lake. Thus, the isotopic composition of the endogenic aragonite is calculated based on the equilibrium fractionation for the aragonite-water system, modeled as:

$$1000 * ln\left(\alpha_{Arag-H_2O}\right) = 17.88 * \left(\frac{10^3}{T_W}\right) - 31.14 \qquad (31)$$

where α_{Arag-H_2O} is the equilibrium fractionation factor for the aragonite and water (Kim et al., 2007), and T_W is the temperature of the water. The value for the equilibrium fractionation factor is related to the isotopic composition of the lake water by the following expression:

$$\alpha_{Arag-H_2O} = \frac{1000+\delta_{arag}}{1000+\delta_L} \quad (32)$$

where δ_{arag} is the isotopic composition of the aragonite. Both δ_{arag} and δ_L are given here in the VSMOW notation. The isotopic composition of the sediment is, however, converted into the Vienna Pee Dee Belemnite (VPDB) notation with the equation:

$$\delta_{VSMOW} = 1.03092 * \delta_{VPDB} + 30.92 \quad (33)$$

The *Sensor* submodel calculates the theoretical isotopic composition of aragonite forming in the water column on each simulated day. However, the formation window of aragonite at Castor Lake happens only in early- to mid-summer (April-June) based on observations of whiting events by local residents as well as observations of the timing of carbonate mineral formation in other, similar systems. Additionally, there is a theoretical temperature control on the timing and amount of formation of endogenic sediment each year because of the need of the water column to reach a degree of Ca^{2+} and CO_3^{2-} saturation that is greater than 1 (Koschel, 1997), according to the expression:

$$\Omega = \frac{a_{Ca}a_{CO_3}}{K_{sp}} > 1 \quad (34)$$

where a represents the activity of Ca^{2+} and CO_3^{2-} , and K_{sp} is the aragonite solubility product. The activity of both ions needed for the formation of aragonite sediment is influenced by climate mostly in terms of precipitation and temperature – the former affects Ca^{2+} ion delivery to the lake via groundwater flowing through carbonate bedrock, and the latter is inversely related to K_{sp}. Furthermore, temperature is known to directly influence primary productivity (with temperature increase during spring promoting

greater production), resulting in the enhanced removal of CO_2 at higher temperatures and a shift in the Dissolved Inorganic Carbon (DIC) equilibrium towards the CO_3^{2-} species (Kelts and Hsü, 1978). Finally, temperature is related to evaporation amounts, which also directly affect the concentration of Ca^{2+} ions in the water column. Thus, aragonite forms throughout the summer due to the aforementioned physicochemical and biological processes which are directly affected by changes in hydroclimate, but have considerable complexity and uncertainty associated with them.

To account for the uncertainty in both the timing and length of the period of the year in which aragonite forms, the *Sensor* submodel randomly selects the moment of aragonite formation season onset as well as its length (both variables represented as days of the year). In this way, the yearly variability in the timing of aragonite formation can be addressed on long simulations (in century to millennial timescales) by the averaging of several realizations of the same time period in which all other inputs remain constant and these timing variables are sampled from a determined normal distribution of plausible values (*see* **Model Calibration)**. Similarly, yearly variability exists in mixing depth values (i.e., depth of shallow lake reservoir) of the water column during the warm season, which in turn has a direct impact on the formation of aragonite (it is in the epilimnion where the inorganic crystal formation takes place). An analogous algorithm is utilized to address this source of uncertainty as for the timing of formation, to similarly determine the extent of the influence the yearly stratification variability has on the resulting isotopic composition of the sedimentary archive.

4.3. Archive and Observation Submodels

The objective of the *Archive* submodel is to represent the processes of sedimentation and surficial sediment re-suspension and mixing that occur on the lakebed. In general terms, the *Archive* submodel takes the output from the *Sensor* submodel (i.e. theoretical isotopic composition of sediment) and turns it into a synthetic, simulated value comparable to one that would be actually obtained from measurements of a sediment core. Due to the temporal resolution of the sediment core measurements (yearly to decadal in most cases), the *Archive* submodel creates one $\delta^{18}O$ value for each simulated year in order to smooth the model data and make it more comparable to actual measured records. Additionally, in order to account for sediment re-suspension and bioturbation, a trailing average of, in this case, 10 years is applied to the data.

Finally, the *Observation* submodel is meant to represent the uncertainties that exist in the measurement of the *Archive* data in real sediment cores, in order to facilitate the comparison between modeled and real proxy data from a sedimentary archive. To this end, analytical uncertainty from carbonate sediment (±0.2‰) was utilized as a confidence interval for the calibration and reconstruction experiments.

4.4. Water Sample Collection and Analysis

Water samples were collected for oxygen isotope analyses from the surface of Castor Lake, as well as from wells in the catchment. Water isotope data from CE 2005-2018 were previously reported by Steinman et al. (2019). The samples were collected following standard procedure, by rinsing high-density polyethylene bottles three times

with samples water and then filling and capping them underwater. After being stored in cool (~4 °C), dark conditions, isotopic ratios were measured either at the University of Arizona (UA) Environmental Isotope Laboratory on a gas-source ratio mass spectrometeror at the Indiana University Purdue University Indianapolis (IUPUI) Department of Earth Sciences on a Picarro L2130-I Analyzed coupled to an autosampler and high-precision water vaporized unit. At UA, Oxygen isotope ratios were measured by equilibrating samples with CO_2 gas at 15 °C in an automated equilibration device coupled to the mass spectrometer. Precision was of 0.9‰ or better on the UA measurements, and 0.1‰ for the IUPUI measurements.

4.5. Model Inputs

The *Environment* submodel uses meteorological data in order to forward model daily $\delta^{18}O$ values in the lake sediment. In this study, a compilation of approximately 120 years of daily climate data was used as model input in order to calibrate, validate and utilize the model for quantitative paleoclimate reconstructions. Daily climate data was compiled from four different sources in order to obtain a complete record that captures daily, seasonal and decadal variability of the regional climate in and around the catchment of Castor Lake: two stations from NOAA National Centers for Environmental Information (NCEI): Conconully (1900-2019) and Omak (1910-2019), the Omak station from the Pacific Northwest Cooperative Agricultural Weather Network (AgriMet) and 14 years of in-situ weather data from a Campbell Scientific weather station (Figure 3; see Steinman et al. (2010b) for specific documentation on in-situ weather data collection).

This latter source was used as a basis for rescaling air temperature, precipitation and relative humidity from the other datasets in order to obtain a corrected, 20th century timeseries of daily weather data for the Castor lake catchment (20th Century refers to the period of 1900-2019 throughout this text). Rescaling of the weather datasets were done using linear regressions during overlapping periods and then correcting the older dataset with the obtained linear relation. For air temperature, the AgriMet dataset was regressed onto the NCEI data over the overlap period of 1989-2018 in order to correct values of the longer timeseries (NCEI data; Figure 4) with the fitted linear model. Subsequently, a similar process was carried out by regressing the weather station (Castor) data onto the timeseries from the first correction, in order to obtain the complete 20th Century temperature data as corrected with the Castor Lake weather station. Relative humidity data was absent from the NCEI datasets and therefore only the second linear correction was applied for the AgriMet data. To fill in the complete time period of 1900-1989, daily averages were utilized from the corrected data that spans 1989-present. Lastly, in the case of precipitation, corrections were applied to daily precipitation amounts on the basis of differences in monthly precipitation amounts. Thus, total precipitation for each month of the year was calculated for all three timeseries (NCEI, AgriMet and the weather station data) so that rescaling factors (i.e., monthly precipitation amount ratios) could be applied to the timeseries. Precipitation values were not corrected utilizing linear models as their fit is usually not good enough to provide a sound statistical trend, due to the high spatial heterogeneity of precipitation in the area, and the amount of days with no precipitation, which skew the relationships. None of the remaining climate variables (i.e., solar

irradiance, wind speed, etc.) were available from these sources and therefore daily averages from the Castor Lake weather station data were applied to the entire period of 1900-2005.

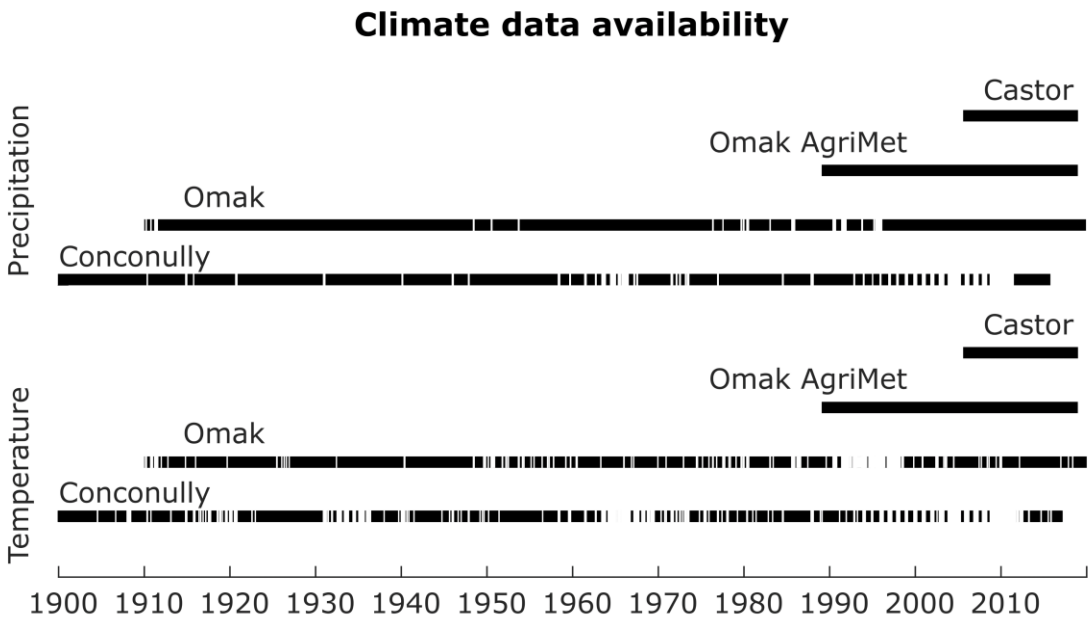

Figure 3. Availability of climate data from weather stations in the vicinity of the Castor Lake catchment. The climate data compilation was based on the Castor weather station data, with which other datasets were corrected or validated before their addition to the compiled dataset. Omak corresponds to stations GHCND:USC00456121; GHCND:USW00094197 and GHCND:USC00456123 and Conconully corresponds to station GHCND:USC00451666 from the NOAA Climate Data Online dataset. Omak AgriMet data obtained from Bureau of Reclamation's Cooperative Agricultural Weather Network (AgriMet) network of climate data for Omak (station name: omaw).

Precipitation $\delta^{18}O$ values were obtained from the Online Isotopes In Precipitation Calculation (waterisotopes.org; Bowen, 2015; Bowen et al., 2005; Halder et al., 2015) and were interpolated to daily values. Additionally, 14 years of continuous lake level and lake water temperature data from Solinst Leveloggers deployed in Castor Lake were utilized for calibration (lake-level data; Figure 5) and as inputs for the *Sensor* submodel

(water temperature data). Lastly, 44 water $\delta^{18}O$ measurements were taken at various times through the 2005-2019 period, also utilized for model calibration and validation (Figure 5).

Lake surface area, volume and depth relationships were obtained from high resolution bathymetric data, surveyed in Castor Lake in the summer of 2019, by contouring the basin from depth and coordinate datapoints and produce a three-dimensional model of the lake basin in ArcGIS. In this way, surface area and water volume values were calculated for lake level increments of 20cm. Based on the U.S. Department of Agriculture regional soil report maps (Steinman et al., 2010a, 2010b), specific soil types and their areas were utilized to calculate a weighted average of available water capacity for the catchment (AWC). Finally, historical lake-level estimates from satellite images and aerial photographs were obtained by comparing the bathymetric data with the lake's surface area at the time the photograph was taken (Steinman et al., 2013).

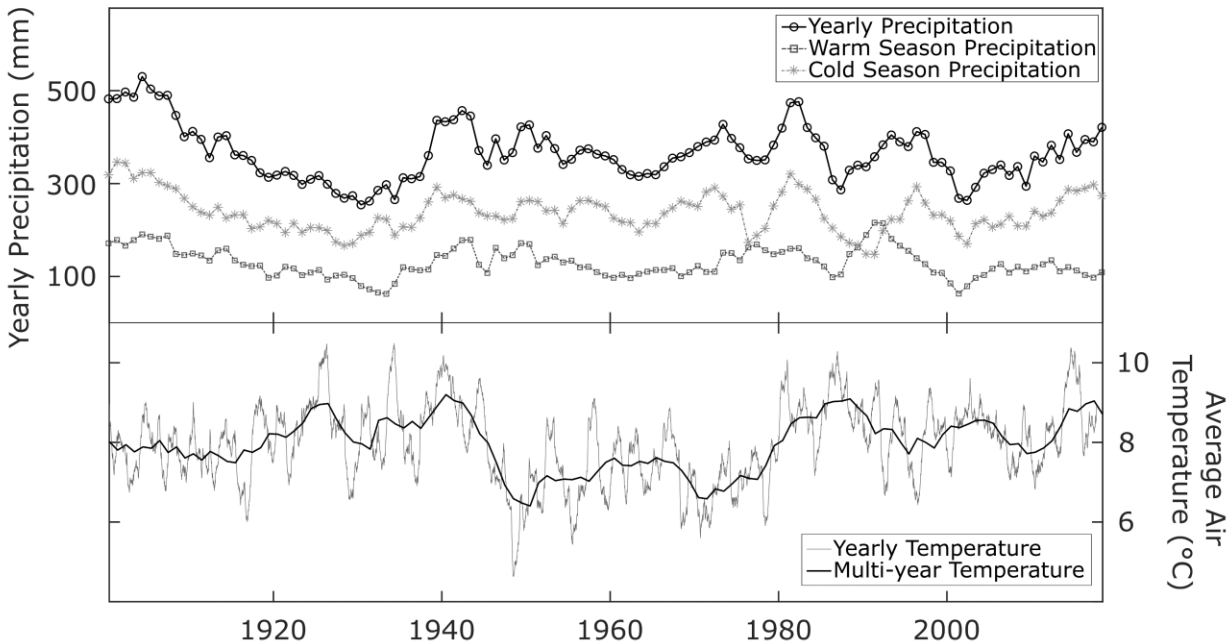

Figure 4. Summary of compiled Precipitation and Air Temperature data for the 20th Century for the Castor Lake catchment, based on the sources in Figure 3. Top: Total yearly precipitation amounts, as well as cold season (Oct – Mar) and warm season (Apr – Sep) amounts. Note the pronounced seasonality in precipitation – cold season precipitation (mostly as snow) dominates the hydrology of the system and the regional water balance. Bottom: 4-year moving average of yearly mean temperatures through the 20th Century (solid black line); 365-day moving average of mean daily air temperatures (grey line).

4.6. Model calibration

In order to determine the numeric values of the four parameters of the *Environment* submodel, an iterative calibration process based on a Monte Carlo approach was carried out in which 100 realizations of the model were run through the time period of the compiled climate data with randomly varying values for one of the parameters *a*, *b*, C_{IN} and AWC_{mod} at a time. Due to the non-linearity of the relationships between parameter values and model outputs (i.e. modeled lake level and sediment isotopic composition), the parameters were calibrated separately and iteratively, therefore

maximizing the goodness of fit between modeled variables and observations (lake level measurements from 2005-2019 and observed $\delta^{18}O$ from Castor Lake sediment core). The criteria utilized to determine the best parameter value for a certain 100-iteration Monte Carlo simulation was based on the minimization of mean-differences and root mean squared errors (rmse) from the modeled and observed datasets. Starting ranges in which optimal parameter values might be were estimated by maximum and minimum values for the outseepage parameters in several lakes (Rosenberry et al., 2015), from previous estimates in monthly-timescale models for C_{IN} (Steinman et al., 2010a) and from half to double the soil water capacity for AWC_{mod}. Thus, for each calibration, constant values were set (as the mean of the parameter value range) for three of the four parameters. The fourth parameter – the one to be calibrated – would be randomly sampled from the uniform random distribution of parameter values and an optimum was determined as the model run that yielded the lowest combined rmse for modeled vs. observed lake level (for the period of 2005-2019) and modeled vs. observed isotopic composition of sediment (1900-present). This process was repeated iteratively for each of the four parameters until convergence in the iterative results was achieved. Convergence was determined for this study as a difference of less than 1% between the last iteration's optimum parameter value and the second-to-last iteration's optimum parameter value. It is important to note that the chosen set of parameter values after the calibration process do not represent the optimal values for lake level or sediment $\delta^{18}O$ composition individually but are instead a compromise that minimizes error for both of these variables simultaneously.

Once the baseline values of the four parameters described above were determined, a second calibration process was performed to assess the uncertainty of carbonate sediment formation in terms of timing, duration, seasonality and spatial distribution within the water column. To do this, a similar procedure to the first calibration was applied, in which the values for onset of "warm" season (day of the year in which aragonite starts forming in the water column) and duration (number of days in which aragonite is produced) were randomly varied – within normal distributions – between endmember dates chosen on the basis of field observations and documentation of whiting events (Steinman et al., 2010a). Also, the mixing depth of the epilimnion during the stratified season was modified using a normal distribution, with a mean approximately equal to the observed value from water column thermal surveys, to simulate variations in thickness of the shallow water layer (as this is the water body in which aragonite is formed). To calibrate the values of these uncertainty variables, which correspond to the *Sensor* submodel, sediment $\delta^{18}O$ outputs from the model were compared with the average measured $\delta^{18}O$ value from the Castor Lake high-resolution $\delta^{18}O$ record (Mark, 2021). After this second calibration step, a range of uncertainty variables for timing and depth of aragonite formation was determined, from which the reconstruction simulations could randomly sample. This is considered more realistic than setting a singular value, since these conditions change every year depending on stochastic or deterministic climate-dependent processes. The uncalibrated and calibrated values for this assessment of uncertainty is summarized in Table 2.

4.7. Instrumental period simulations

Model simulations were run in order to produce lake level and sediment $\delta^{18}O$ simulations for the period of 1900-2019, during which daily weather data was compiled (Figure 4). The model was initialized with order-of-magnitude approximations for the volumes for each water reservoir and isotopic composition, and then a period of 20 years of equilibration was run in which average daily climate values were applied as inputs and steady state was observed. After this "spin-up" period (Figure 5), simulations were started on the 1st of January 1900. Ranges for aragonite formation timing and mixed layer depth were randomly sampled from normal distributions obtained from the calibration of these variables, and the values for the first set of parameters (a, b, C_{IN} and AWC_{mod}) were kept constant in all simulations. The mean values for the 20th Century model runs, as well as the observed lake-level and water $\delta^{18}O$ data with which the model was calibrated, are shown in Figure 5.

4.8. Paleoclimate interpretation simulations

In order to quantitatively assess the climatic context in which a certain horizon of carbonate sediment from the lake formed and deposited, a forward modeling process was utilized in which randomized variability to the climate inputs into the *Environment* submodel was introduced, and the resulting *Archive* values were compared with measurements of the actual sediment record from Castor Lake. This interpretation methodology was applied in order to reconstruct multi-decadal to century-scale periods in the Holocene sedimentary record. To this end, a suite of Monte Carlo simulations was run in which the model simulated the 20th century (after the 20 years of equilibration) and,

subsequently, a change was applied to one or more of the climate variables: precipitation, air temperature and/or relative humidity. This change was modeled using a modified version of the ~120-year input climate dataset in which the order of the data was randomly modified to produce a new, synthetic climate dataset to which climate alterations were applied. The re-ordered data was constructed by randomizing an assortment of 10-year blocks of the original timeseries (in order to conserve some of the sub-decadal-scale variability in the data).

Each realization for the paleoclimate reconstruction consisted of four stages: a 50yr equilibration period, a 20th Century simulation with the compiled climate data, a simulated modern (termed "average modern", Figure 7.E) period of the same length with the randomized climate data, and a "reconstruction" simulation in which the precipitation, temperature or relative humidity values were altered using the randomized climate data utilized for the third stage of the simulation (Figure 7.F). The changes for temperature and precipitation were done seasonally: different changes were applied to 'warm' (April – September) and 'cold (October – March) seasons independently (Figure 7.B, 7.C). Relative humidity values were modified directly as a proportion of the actual value for the simulated day (as a percentage) and temperature values were modified by a certain number of temperature degrees, independent of the actual value of the day's air temperature (Table 3). In the case of precipitation modifications however, due to the pronounced seasonality of precipitation in the region (modifying both warm- and cold-season precipitation by the same proportions would result in cold-season dominated outcomes) as well as the high inter-annual variability in precipitation totals, a different

approach was taken than a direct daily percent change in the precipitation amounts. For every year, the percent modifications for warm- and cold-season precipitation (Table 3) were first multiplied by the ratio of warm- or cold-season precipitation vs. total precipitation for that year, and that value was the one by which daily precipitation for the corresponding season was modified. In this way, individual years would see precipitation alterations proportional to their total precipitation amounts (independent of intra-annual seasonality) and inter-annual precipitation variability was conserved on each realization.

For the execution of the reconstruction experiments, 1000 realizations of the four simulation stages ("spin-up, "20th Century", "average modern" and "reconstruction") were produced (Figure 7). For each realization, a unique set of climate scenarios was randomly chosen from the distributions shown on Table 3. The utilization of this iterative methodology eliminates the variability caused by instrumental climate data noise in the daily to interannual timescales (in the "average modern" and "reconstruction" stages) by averaging realizations with re-ordered timeseries and allowing for the determination of century and millennial scale values in the resulting simulated sediment isotopic compositions (Steinman et al., 2015). The experiments provided three separate products: (1) an averaged 20th Century simulation, in which uncertainty due to sediment formation timing and amounts were taken into account and then compared to measured 20th Century $\delta^{18}O$ measurements (Mark, 2021); (2) a "modern averaged" century-scale value for sediment $\delta^{18}O$ composition in which shorter-timescale variations are eliminated through the averaging of the randomized climate datasets; and (3) a "reconstruction" sediment $\delta^{18}O$ value which, by analyzing a specific group of climate alterations (to precipitation,

temperature and relative humidity), yielded insight into the climate scenarios in which specific ^{18}O signatures in sediment could theoretically be produced and recorded. Two sets of Monte Carlo simulations were produced: the first, with wide ranges of random climate variability that both increased and decreased relative humidity, temperature and precipitation, and which gave a general approximation as to the order of magnitude of the changes required to produce the "target" sediment reconstruction value (in this case, the early Holocene maximum of $\delta^{18}O$); the second, which utilized narrower ranges of climate variable alterations chosen from the results of the first experiment, which allowed for the further constraining of the goal climate scenarios form which the early Holocene isotopic composition values were obtained (*see* ***Early-Holocene paleoclimate reconstruction***).

5. Results and Discussion

5.1. Calibration Results and 20th Century Simulations

After calibration, the *Environment* submodel output was compared to lake level measurements from satellite images and levelogger measurements. Figure 5 shows these results through the 20th century and into the Castor Lake weather station and monitoring period. Two main drought periods in the 20th century are visible in the lake-level reconstruction for Castor Lake: the first one approximately in the 1925-1935 period (from which no lake level data is available) and the other from the late 1980s until the mid-1990s. There is evidence from aerial photos of a considerable drop in lake level during the latter drought period (Figure 5.A), as the lake reached its minimum observed depth of 10m. However, this represents a snapshot of time, and the extent of lake level drop might

have been lower. Markedly, the lake-level reconstruction accurately reproduces the estimated lake levels from the satellite imagery, with the exception of two values (from 1945 and 1952). This could be a result of inaccuracies in climate data estimates from that time, unaccounted-for uncertainty in the lake level estimates, and/or failure of the model to represent the real-world lake system during lake-level lowstands.

The calibration results of the aragonite-formation uncertainty variables (onset and duration of the aragonite-formation season and depth of the shallow lake reservoir; Table 2) show that only the onset of the aragonite-formation season has a significant control on the sediment $\delta^{18}O$ values and that the formation of sediment, as simulated, must start much earlier than expected (24th of April ± 10 days, instead of the estimated 23rd of May ±38 days). Because the new, calibrated distributions for the three analyzed variables were picked based on the comparison of modeled vs. observed 20th Century (1900-2019) sediment $\delta^{18}O$ values (averaged over the entire time period), this shift in the aragonite-formation season shows that the modeled water $\delta^{18}O$ values in which the resulting aragonite isotopic compositions are closest to reality are those that correspond to the spring snowmelt, which occurs approximately during this time. This finding supports previous evidence that it is indeed these volumetric fluxes to the lake that control not only the year's water balance but also the characteristic isotopic composition of the lake water, which later in the year experiences mostly enrichment from kinetic fractionation due to evaporation and the lack of warm-season precipitation. The "new" ranges of variability for the three variables analyzed in this second calibration procedure

correspond to the values that were utilized for all subsequent analyses, including 20th Century simulations and quantitative paleoclimatic reconstructions.

Table 2. Summary of aragonite formation uncertainty variable distributions before and after calibration. Note the change in ranges for the timing of the onset of the aragonite formation season after calibration, from an assumed start at around mid-to-late may, to approximately a month prior.

Uncalibrated Values						**Calibrated Values**					
Mixing depth (cm)		**Start of Aragonite Formation Season (Day of Year)**		**Length of Aragonite Formation Season (Days)**		**Mixing depth (cm)**		**Start of Aragonite Formation Season (Day of Year)**		**Length of Aragonite Formation Season (Days)**	
Mean	2σ Range	Mean	2σ Range	Mean	2σ Range	Mean	2σ Range	Mean	2σ Range	Mean	2σ Range
600	300	143	±38	99	±22	606.14	±301.98	114	±10	95	±21

In general, the *Environment* model accurately represents the water balance dynamics in the lake system. Uncertainties in the compiling and correction of the climate datasets, coupled with lack of observational data of lake-level change through the 20th Century, might be responsible for inconsistency between modeled and estimated/observed lake-level data. When the model is run only through the period of in-situ weather station data availability (2005 – 2019), it most accurately reproduces lake-level changes and water isotopic compositions, which supports the hypothesis that precipitation amount uncertainties on the compiled weather data are what drive the deviation between modeled and observed lake levels. Figure 5.A shows that the model generally reproduces the multi-year trends of lake level well; however, high and low stands are not as accurately reproduced by the simulations as the more average trends. It is possible that these short-lived events of anomalously high or low lake levels are not

successfully predicted by the simulations due to heterogeneities in the sedimentary basin that the outseepage subroutine could not resolve or because of precipitation events that might have happened only high in the Castor Lake area and therefore were not recorded by the proxy weather datasets utilized for most of the 20th Century timeseries which come from weather stations located at lower altitudes and which are somewhat drier overall. However, as the interest of this modeling study is the characterization of century to millennial timescale changes in water balance and not the prediction of the system's response to dry or wet years, and because longer-term lake level fluctuations are indeed captured by the simulations, these discrepancies were not considered as an issue. Furthermore, this is not a pristine system and human alterations of the landscape have been present for the entire analyzed period of this study, thereby adding to the complexity of the hydrologic system and having an influence on the amounts, timing and even existence of the assumed hydrologic fluxes to and from the lake.

Observed surface water $\delta^{18}O$ values were generally well predicted by the model simulations (Figure 5.D), indicating that the calibration through the comparison of model outputs with lake-level observations and sediment isotopic compositions successfully constrained the isotope dynamics of the lake. The goodness of fit of the water $\delta^{18}O$ samples in relation to the model, therefore, may be interpreted as a validation experiment that showcases the accuracy of the physics behind the hydrology of the system and its relation to the isotope mass-balance in the lake. Water sampling in the 2006-2010 period was considerably more thorough and therefore provides higher temporal resolution, demonstrating isotopic enrichment of the epilimnion as the summer progressed. This is

especially apparent in the summer of 2006 in Figure 5.D, when the summer enrichment is documented by a total of eight samples taken from May through October of that year, and the $\delta^{18}O$ trends of the model and measurements are similar. The lake was sampled along the northwest shoreline in the 2016-2018 field seasons, at a location of periodic surficial inflow and shallow groundwater recharge to the lake. Because of this, these samples are suspected to not be representative of the entire epilimnion, as most of the groundwater is sourced from spring snowmelt and is therefore much more depleted than the average composition of lake water, which could explain why the modeled $\delta^{18}O$ deviates from measured values during this time interval.

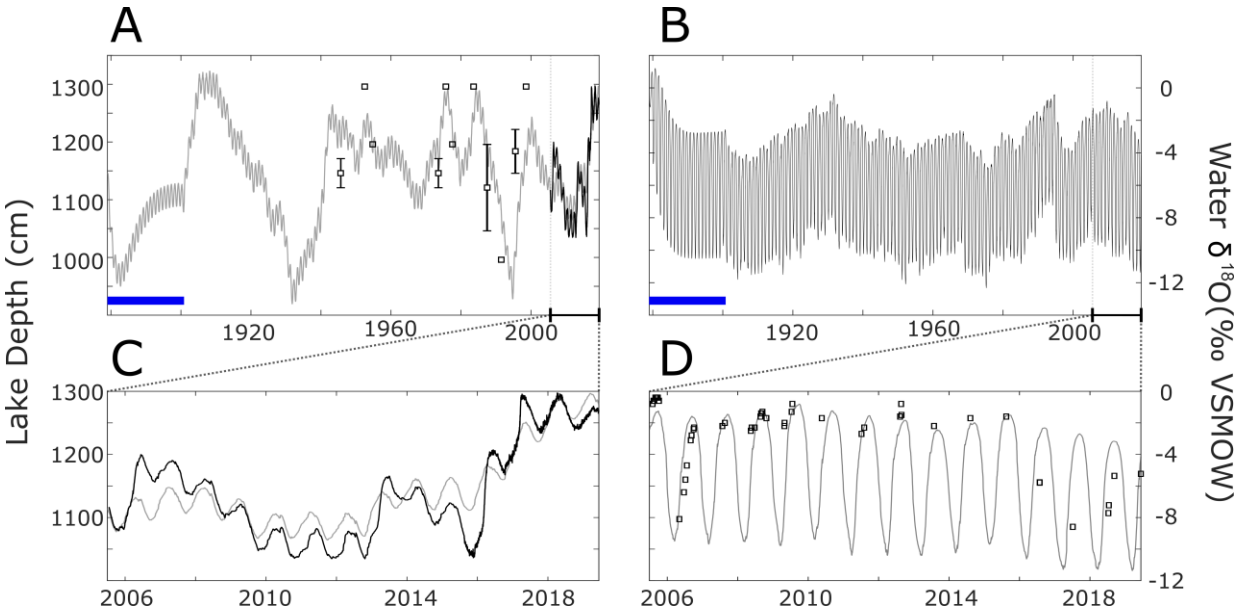

Figure 5. Summary of Environment submodel outputs for 20th Century simulations. Thick blue line represents "spin-up" period in which only average daily data was utilized in order to equilibrate the model. **A:** Entire 20th Century modeled lake-level (solid grey line), estimated lake level values based on satellite and aerial photographs, with estimated uncertainties (black boxes) from Steinman et al. (2013), and observed lake level from on-site leveloggers (solid black line). **C:** 14 years of simulated (grey line) and observed (black line) lake-level data. **B:** Entire 20th Century modeled shallow water $\delta^{18}O$ values. **D:** 14 years of simulated (grey line) shallow water $\delta^{18}O$ values, and measured $\delta^{18}O$ from water samples (black boxes). Note the enhanced resolution of sampling in the first five years of monitoring, in which progressive enrichment of the epilimnion through the summer months is evidenced.

Sediment $\delta^{18}O$ was also reconstructed for the instrumental period of the 20th Century in order to assess whether the *Sensor* and *Archive* submodels could accurately reproduce measured Castor Lake $\delta^{18}O$ data. Century-scale average values for both the measured and modeled records are -4.8‰ and -4.9‰, respectively (Figure 7.D), indicating that the modeled average value for the length of the entire 20th Century record falls within the 2σ analytical uncertainty range of the measured values (±0.2‰). Nonetheless, while multi-decadal trends in the modeled and measured archives are similar, shorter time-scale variations exhibit significant discrepancies, particularly over two intervals: a wet period around the first two decades of the record (1900-1920) and a dry period towards the late 1990s. Additionally, two highly negative excursions occur in the Castor $\delta^{18}O$ record around the years of 1940 and 1960, which are not concurrent with significant increases in precipitation amounts on those or immediately preceding years (Figure 4), and which be due to other processes that have not been accounted for in this modeling exercise. These discrepancies could be a result of uncertainty of the weather data from the early parts of the century, relative insensitivity of the proxy to these decadal-scale climate events, or high variability in the sedimentation rates and inter-annual sediment formation rates. In order to investigate these differences, the observed and modeled sediment proxy records were compared to a tree-ring record of winter precipitation (SUG) (Wise and Dannenberg, 2017; Figure 6). SUG record is shown to track the cold-season precipitation record, indicating that uncertainty associated with this data is unlikely to be the cause of the disagreement between modeled and observed sediment isotopic compositions. As proposed by Steinman et al. (2013), the Castor

record is mostly dependent on winter precipitation, and other climate variables are of secondary importance. However, the observed Castor record for the last 100 years exhibits less decadal-scale variability than both the SUG record and the winter precipitation dataset (Figure 6), which could support the hypothesis that this sedimentary system is not sensitive enough to decadal or shorter perturbations or changes in winter precipitation. An additional possibility is that during dry periods reduced delivery of Ca^{2+} ions limits carbonate mineralization, leading to the underrepresentation of dry intervals in the sediment archive. This could be the case for the large discrepancy between the modeled and observed $\delta^{18}O$ values in the late 1990s, as well as a smaller departure during the 1960s (Figure 6). Lastly, the *Archive* submodel may not be capturing sediment resuspension or bioturbation effects that are effectively averaging longer periods of time than the 10 years accounted for by the trailing average. Therefore, a deeper investigation of the mechanisms that remobilize and homogenize the surficial sedimentary layers should be undertaken in order to further constrain the *Archive* submodel.

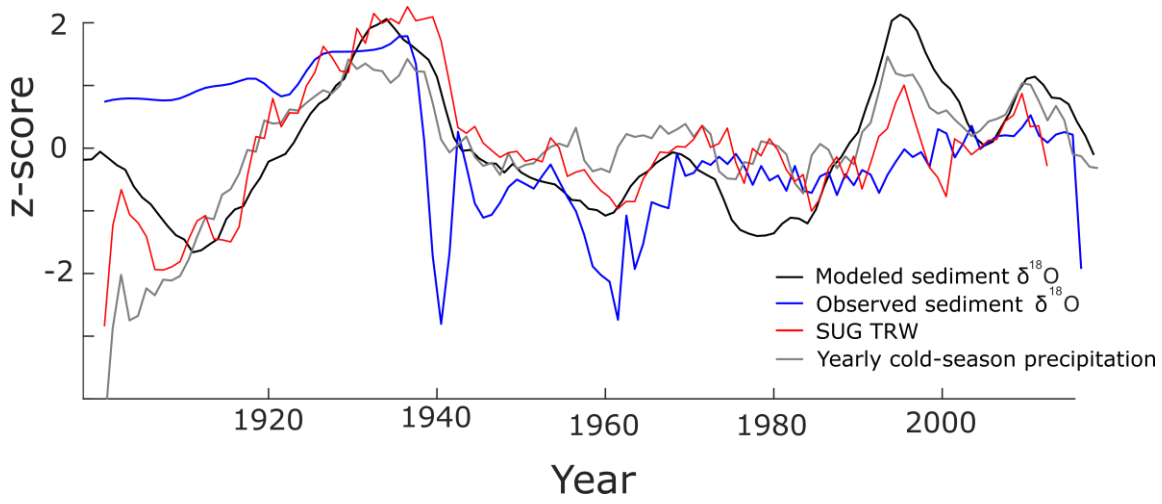

Figure 6. Z-scored timeseries of: 10-year trailing average of modeled yearly $\delta^{18}O$ composition of sediment (Modeled sediment $\delta^{18}O$), observed high-resolution (1 year) Castor Lake sediment isotopic composition (Mark, 2021), 10-year trailing average of total tree-ring width from SUG record (Wise and Dannenberg, 2017), and 10-year trailing average of compiled 20th Century (1900-2019) cold-season (October-April) precipitation amounts.

5.2. Early Holocene paleoclimate reconstruction

In order to quantitatively reconstruct the hydroclimatic conditions during the early Holocene ("target") period, two suites of Monte Carlo simulations were run in which five climate variables were modified (Table 3; *see* **Paleoclimate Interpretation Simulations**). The $\delta^{18}O$ record from Steinman et al. (2019) shows a maximum value for Early Holocene sediment $\delta^{18}O$ of -2.4‰ ± 0.1‰ (Figure 5.A; red star; 500 year lowpass filter applied). Initially, the set of climate modification values (% warm-season precipitation, % cold-season precipitation, ℃ warm-season temperature, ℃ of cold-season temperature and % relative humidity) from model realizations in which the sediment $\delta^{18}O$ value from the "reconstruction" stage fell within the 2σ analytical uncertainty range (± 0.2‰) of this Early Holocene value were recorded. Results of this first assessment were

used to produce normal distributions for the five variables that were utilized as the basis for the second run of simulations, in which more constrained ranges for the climate variables were applied in order to refine the reconstruction (Table 3). Note that the modifications for daily air temperatures were calculated in absolute values (degrees Celsius), while relative humidity and precipitation were changed relative to their original values (as percentages). Panel C of Figure 5 shows the statistical spread of the five climate variable modifications that successfully reproduced values the Early Holocene sediment $\delta^{18}O$ maximum.

Table 3. Summary of climate variable modifications for the quantitative reconstruction of Early Holocene $\delta^{18}O$ values. The 'reconstruction' stage of the iterative model simulations randomly sampled from these normal distributions in order to modify the climate variables and assess what impact these modifications had on the resulting mean $\delta^{18}O$ values in the modeled proxy record.

Climate Variable	**Modification 1st Run**	**Modification 2nd Run**
Warm Season Precipitation	0 % ± 30 %	-0.01 % ± 0.19 %
Cold Season Precipitation	0 % ± 30 %	-0.18 % ± 0.06 %
Relative Humidity	0 % ± 10 %	-0.06 % ± 0.035 %
Warm Season Temperature	0 ˚C ± 2.0˚C	+0.99˚C ± 0.5˚C
Cold Season Temperature	0 ˚C ± 2.0˚C	-0.82˚C ± 0.9˚C

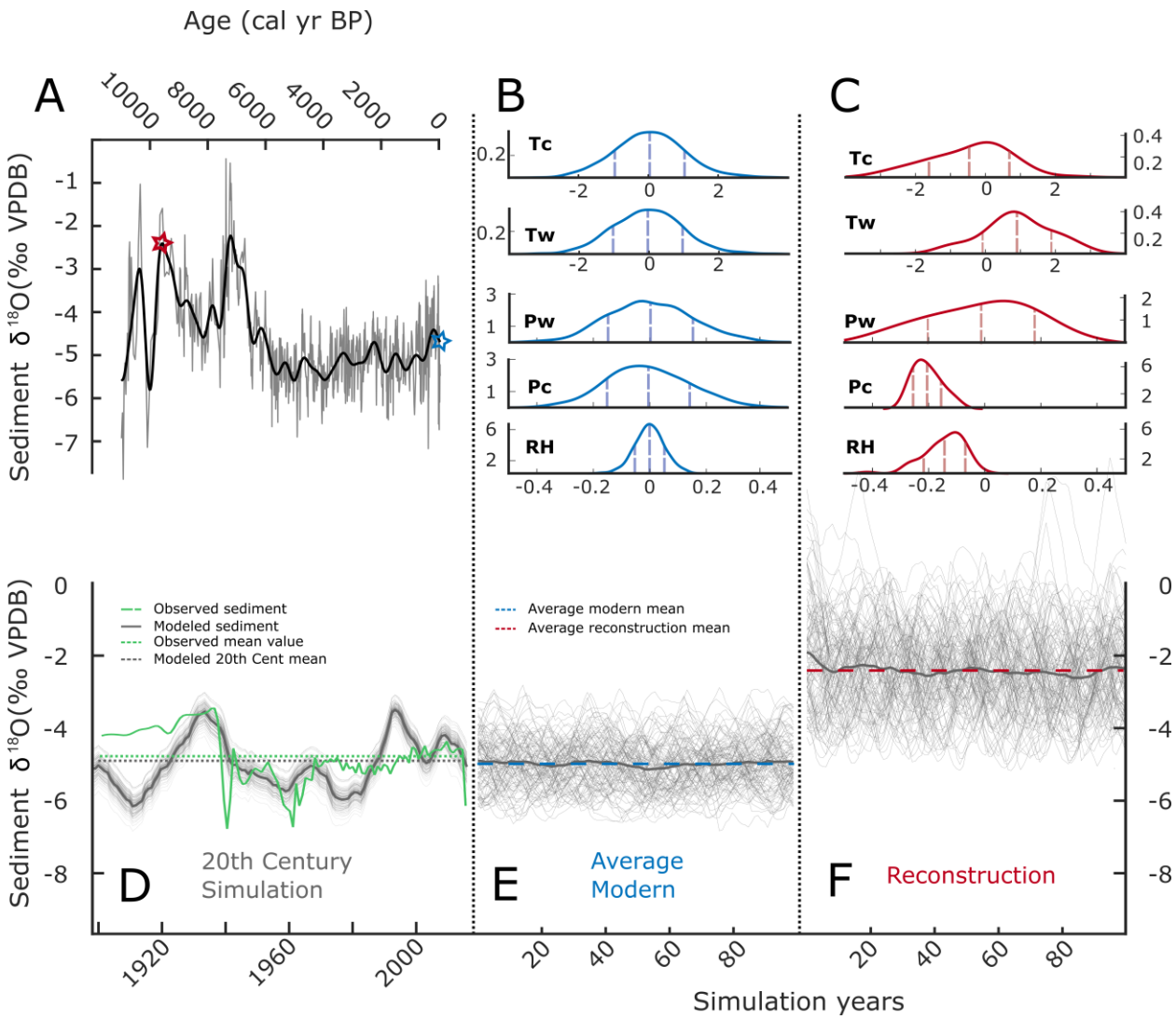

Figure 7. Summary of results for the quantitative paleoclimate reconstructions based on the reproduction of measured $\delta^{18}O$ values from the Castor Lake proxy record. **(A)**: Holocene $\delta^{18}O$ record from Castor Lake carbonate sediment modified from Steinman et al., (2019), showing the entire record (grey line) and 500-year low-pass filtered time series (black line). Red star indicates Early *You* Holocene $\delta^{18}O$ maximum in the record, chosen in this study as the "target" value for paleoclimate reconstruction (~ -2.4‰). Blue star indicates mean modern $\delta^{18}O$ values in surficial sediment. **(B)**: Probability density estimates for climate variable modifications (in ˚C for Tw and Tc, and relative change for Pc, Pw and RH) necessary to obtain average modern century-scale $\delta^{18}O$ values in the modeled sediment (Blue star in Panel A; dashed blue line in Panel E). Tc= Cold-season temperature (Oct – Mar); Tw = Warm-season temperature (Apr – Sep); Pw = Warm-season precipitation; Pc = Cold-season precipitation; RH = Relative Humidity. **(C)**: Probability density estimates of climate variable modifications necessary to obtain the "target" $\delta^{18}O$ value from the Early Holocene maximum (Red star in Panel A; dashed red line in Panel F). Note the wide ranges of probability distributions for both warm and cold season temperature and warm season precipitation values, and the narrower ranges for cold season precipitation and year-round relative humidity. Panels D, E and F showcase the three stages of the reconstruction simulations: **(D)**: 20th Century simulated aragonite $\delta^{18}O$ records produced by random sampling of aragonite formation uncertainty variables (Table 2; thin grey lines); 10-year trailing average of mean modeled sediment $\delta^{18}O$ values from all simulations (thick grey line); observed, yearly resolved $\delta^{18}O$ record from Castor Lake sedimentary record modified from (Mark, 2021; solid green line). Average $\delta^{18}O$ values for both modeled and observed datasets shown as horizontal dashed lines. **(E)**: Average modern simulations with random sampling of aragonite formation uncertainty and

randomized re-ordering of climate data (thin grey lines); mean $\delta^{18}O$ timeseries for all 'Average Modern' simulations (thick grey line); average 100-year $\delta^{18}O$ value for the mean timeseries (note that the randomized re-ordering of climate series and aragonite uncertainty creates a wide range of noise that is cancelled by the averaging of all the iterations, yielding the century-scale proxy value under these average climatic conditions). **(F)**: Simulation results from model realizations which produced 100-year average $\delta^{18}O$ values within uncertainty ranges of measured Early Holocene maximum (red star). The spread of climate variable modifications necessary to produce these realizations is shown in Panel C. Mean modeled sediment $\delta^{18}O$ from these realizations (thick grey line) and 100-year average (dashed red line) are shown. Note the reproduction of the Early Holocene $\delta^{18}O$ maximum "target" value (~-2.4 ‰).

Quantitative reconstructions of the Early Holocene (~10000 years B.P) $\delta^{18}O$ maximum from the Castor Lake sedimentary record suggest that reductions of approximately 21% ± 5% in cold-season precipitation amounts, and of 14% ± 7% year-round relative humidity are necessary conditions in order to obtain a $\delta^{18}O$ value as the one observed from this time. All other climate variable modifications (warm and cold season air temperatures and warm season precipitation amounts) show a considerably small impact in the isotopic compositions of the resulting sediment, as their spread spans both positive and negative values and has uncertainty ranges that are larger than the considered scenarios. The averaging of the "modern average" stages for the 1000 realizations of the second set of Monte Carlo experiments shows how the model successfully reproduces the average modern value of sediment $\delta^{18}O$, as determined from the high-resolution record of surficial sediment from Castor Lake (Mark, 2021). Additionally, due to the randomized reordering of climate data for these simulations, the averaging of 1000 different timeseries produces a dataset that represents mean-state conditions as produced by modern climate through the last 120 years (Figure 7.E), regardless of shorter time-scale variability. As modern weather data was used as an input for the model, it stands to reason that no modification to this data was needed in order to produce the modern proxy values (Figure 7.B). Therefore, in agreement with the

conclusions of prior studies, (Steinman et al., 2010a, 2012, 2013), the Castor Lake d18O record appears to reflect relative changes in winter moisture balance, and cannot be reliably used for inferring other paleoclimatic phenomena such as temperature change.

6. Conclusions

Stable-isotope proxy systems from lacustrine sedimentary archives exhibit complex, non-linear relationships with both climate variability and lake or catchment factors that may affect the reservoir's chemistry and hydrology over human and geologic timescales. Because of this, the application of site-specific computational models that characterize the hydrology and isotope dynamics of lakes is informative and advantageous to appropriately infer changes in past climate and untangle these signals from other, non-climate related variability in the lake or catchment. To elaborate on the assessment of these complexities a Proxy System Model (PSM) was designed and tested in order to provide a tool for the characterization of paleoclimate records of heavy Oxygen stable isotopes – as measured in lacustrine carbonate sediments – as they are related to climate variables such as precipitation and temperature. Specifically, this model is capable of transforming input data related mostly to the climatic context of the study area, as well as the geology, vegetation, morphology and other catchment-specific factors, into estimations of water balance (lake level) and proxy value (water/sediment ^{18}O compositions). Through direct comparison between these model outputs (predictions) and measurements of the same variables, the model was demonstrated to accurately reproduce hydrologic and isotopic composition changes in Castor Lake as they respond to

climatic influences. Thus, by appropriately reproducing the hydrology and isotope geochemistry of the lake, the PSM is understood to be able to model the relevant factors that control the isotopic composition of the carbonate sediment that forms in the water column, and therefore to be capable of assessing the climatic conditions in which an observed $\delta^{18}O$ record might have been deposited in the past.

In order to provide consistency with recent PSM studies, the model presented here was divided into four distinct submodels (Dee et al., 2016; Evans et al., 2013) that allow for the separate analysis of the distinct phases in which the sedimentary ^{18}O record is produced in a lake and subsequently observed: the *Environment, Sensor, Archive* and *Observation*. In this way, the physical, chemical and biological processes that influence the isotopic signature of the sediments, and subsequent processes that might influence their measured values, can be individually simulated and characterized. The PSM effectively transforms input data and parameters into lake water balance (lake level) and water isotopic compositions (*Environment* submodel), which subsequently lead to sediment isotopic compositions (*Sensor)* and finally simulated proxy records (*Archive* submodel). Finally, analytical uncertainty is considered in the comparison between simulated and observed records (*Observation* submodel). For simulations of Castor Lake, climate data was compiled and corrected using daily weather timeseries from two NOAA National Centers for Environmental Information (NCEI) weather stations: Conconully (1900-2019) and Omak (1910-2019), the Omak station from the Pacific Northwest Cooperative Agricultural Weather Network (AgriMet; 1989-2019), and an in-situ weather station in continuous operation over the last 14 years (2005-2019; this timeseries served

as a reference to which the other datasets were corrected or scaled). The model was calibrated utilizing 14 years of continuous lake level monitoring data, as well as a sub-decadally resolved $\delta^{18}O$ record from the lake depocenter. Validation was achieved though comparison of model results with lake level estimates from the mid and late 20th Century based on analysis of satellite imagery and aerial photographs, and measurements of water isotopic composition spanning 14 years measured in water samples from the lake.

Two separate calibration experiments were carried out in which the first one aimed to determine values for the four hydrological parameters of the model (related with lake outseepage and shallow groundwater or soil moisture influxes) by iteratively comparing model outputs (lake level from 2005-2019 and sediment $\delta^{18}O$ from 1900-2019) with observed values of the same variables and choosing parameter values that yielded the most realistic simulations. The second calibration experiment was done to assess three sources of uncertainty for the that were considered to influence $\delta^{18}O$ signatures of carbonate sediments at Castor Lake: mixing depth, onset of sediment formation season, and length of sediment formation season. By following a similar methodology to the first calibration, it was concluded that of the three, only the onset of sediment formation season had a discernible effect on the isotopic compositions of the resulting simulated sedimentary records, and that in order to produce ^{18}O records similar to observed, sediment in the model starts forming approximately a month prior to what was assumed (mid-April instead of mid-May). Ranges of variability for the three variables considered in the second calibration were nevertheless kept in order to

propagate the uncertainty that inter-annual variability might have on the resulting carbonate $\delta^{18}O$ record.

Once the model was calibrated, simulations spanning the period of 1900-2019 (termed 20th Century simulations in this study) were produced in order to assess the extent to which the PSM is capable of recreating water balance and sediment $\delta^{18}O$ from climate data inputs alone. Furthermore, these simulation results were compared with independent observations of model output variables that were not considered in the calibration exercises, therefore allowing for model validation, such as lake level estimates from the mid and late 20th Century and water $\delta^{18}O$ measurements. Overall, the 20th Century simulation results were satisfactory as they accurately reproduced seasonal and inter-annual trends in water balance and water isotopic compositions, especially for the period of in-situ weather and water depth observations. However, although the water balance and water $\delta^{18}O$ values are in relatively good agreeance between model outputs and observations, the proxy records differ considerably from one another and there exists a clear trend for the simulated record to exhibit higher interannual and decadal variability than the observed record, even with the applied 10-year trailing average that aims to model sediment re-suspension and surficial mixing. Although multi-decadal trends are similar, shorter timescale discrepancies of up to 2‰ can be observed in the early part of the 20th Century, and of about 1‰ during the mid-1990s. These differences may be related to the stochastic nature of the sedimentary archive in the lake (i.e., sediment formation and preservation), which may be biased toward signals that represent moments in time with hydrological conditions that are beneficial for the abundant deposition of

authigenic aragonite. In this way, even though the isotopic composition of sediment (assumed to be reflective of the water at the time of formation) chiefly represents variability in the precipitation vs. evaporation balance in the lake, its formation depends upon a wide range of biological (e.g., control of primary productivity on DIC species and water pH), chemical (e.g., availability of catchment-derived Ca^{2+} ions) and physical (e.g., temperature dependence of isotopic fractionation in the water-aragonite system) processes that are each differently impacted by inter-annual variability of moisture availability. Therefore, these annual or decadal biases should be taken into consideration for the future interpretation of ^{18}O records from lakes such as Castor Lake. Nonetheless, century- and millennial-scale signals are likely reflective of hydroclimate variability in these timescales.

As an illustration of one of the possible applications that the presented PSM allows for, modeling experiments were conducted in order to quantitatively constrain the hydroclimatic conditions in which the early Holocene (~10000 years B.P) maximum $\delta^{18}O$ value in the Castor Lake sediment was formed and deposited. The methodology utilized in this study follows an iterative approach similar to the calibration process, but in which two Monte Carlo simulations of 1000 realizations, divided into four stages ("spin-up", "20th Century", "average modern" and "reconstruction"), were run in order to produce century-to-millennial timescale mean values that represent what the isotopic signatures in the sediment would look like for a certain combination of climatic changes. These changes were applied to five climate variables: precipitation and air temperature in the warm season (Apr – Sep) and cold season (Oct – Mar), and year-round relative humidity,

by randomly sampling from normal distributions of possibilities for each variable (wide ranges of scenarios for the first set of simulations, whose results informed the second set, allowing for narrower distributions of climatic scenarios). The results from this reconstruction show that reductions of approximately 20% ± 5% in cold-season precipitation and of 14% ± 7% in Relative Humidity were needed in order to obtain the $\delta^{18}O$ value measured in the sedimentary record (~ -2.4‰); additionally, warm season precipitation and air temperature from either season were comparatively unimportant in terms of their influence on the isotopic composition of the sediment, and therefore changes in these variables cannot be resolved or inferred through analyses of $\delta^{18}O$ values in sediment from Castor Lake. These results are in agreeance with previous studies from this and similar lakes, which found that winter precipitation is the strongest control on the system's hydrology and the geochemical signatures of the isotope proxies (Nelson et al., 2011; Steinman et al., 2013b, 2010a).

Although some of the limitations of this study are manifested in the discrepancies between the simulated and observed 20th Century $\delta^{18}O$ records, as well as the fact that such high-resolution monitoring data with which the PSM was be calibrated and validated are not readily available for most lakes, the results of this study are encouraging for the future application of similarly structured models to other proxy systems. Indeed, simpler versions of the PSM presented here have been applied in other studies (Stansell et al., 2020) in order to characterize other lakes' sensitivities to climatic changes and to quantitatively constrain or interpret their stable-isotope proxy records. The wide use of computational modeling and PSMs as tools for better understanding past climate changes

for different types of records and proxies, and for a variety of timescales, is of considerable importance for the constraining of global atmospheric dynamics in the recent and geological past, which in turn is critical knowledge for the continuous improvement of global climate models and the improvement of climate change mitigation policies.

7. Future Work

A conceptual limitation of this study exists in relation to the inherent variability of meteoric water isotopic composition, which likely impacts the baseline values of surficial water isotopic compositions in continental settings. As such, the monthly average values for precipitation $\delta^{18}O$ used in this study are not necessarily representative of isotopic signatures of snow and rainfall as they would have changed through the Holocene. To address this issue, future work should include an assessment of past changes in meteoric water isotopic signature changes and the creation of a time-dependent precipitation $\delta^{18}O$ record through the Holocene, with which the model is run. In this way, simulated mean values in century- and millennial-scale proxy values would more accurately represent reality and a comparison between these simulations and real-world archive measurements would yield higher quality quantitative reconstructions of past climatic change. Nonetheless, the approximations used are deemed to provide a useful representation of the proxy system's dynamics, at least through the 20th Century simulations and the average modern values; additionally, the changes in isotopic composition of precipitation in the past, although significant, would likely not alter the hydroclimate interpretations made in this study in a considerable amount.

Another principal limitation of this modeling study consists on the assumption that the simplified Penman equation for evaporation and catchment evapotranspiration accurately describes these hydrologic outfluxes. This is not necessarily true and because evaporation is the most important hydrologic control on lake water isotopic compositions, further work should go into further constraining its seasonal and interannual variability as it relates to climate and hydrology. Additionally, water column stratification, although some uncertainty was addressed in the calibration experiments, is mostly assumed to be constant in terms of depth and timing of mixing. For these reasons, future work should also include dynamic energy balance considerations, which would be a helpful addition to the *Environment* submodel as they would help parametrize mixing depth and timing, as well as better model evaporation from the lake and the catchment. However, it should be noted that the extent to which mixing depth and timing affect the isotopic signatures of the resulting proxy archive is not entirely known as of yet, and in small systems such as Castor Lake, it might be an irresolvable effect. Comparing evaporation estimations from both Penman and heat balance subroutines would nevertheless be a fruitful exercise to assess the quality of approximations of evaporation achievable with empirical equations, which are considerably more efficient in terms of computational power.

In order to keep with the goals of this modeling study, which proposed the consideration of age model uncertainty in addition to analytical uncertainty from the $\delta^{18}O$ record observations, a Monte Carlo approach similar to the one showcased in the reconstruction procedures should be carried out in which different realizations of the Castor Lake sediment age model are recreated. In this way, comparisons between

simulated and observed geochemical proxies would be better-informed and statistically sound. These comparisons would, in turn, aid in further constraining the confidence intervals of hydroclimate reconstructions made for proxy observations, specially from older samples or stratigraphic horizons. Lastly, the PSM presented in this study should be translated into Python, a free, readily available programming language which represents a higher scientific impact potential for this tool than MATLAB.

8. References

- Abbott, M.B., Wolfe, B.B., Wolfe, A.P., Seltzer, G.O., Aravena, R., Mark, B.G., Polissar, P.J., Rodbell, D.T., Rowe, H.D., Vuille, M., 2003. Holocene paleohydrology and glacial history of the central Andes using multiproxy lake sediment studies. Palaeogeogr. Palaeoclimatol. Palaeoecol., Late-quaternary palaeoclimates of the southern tropical Andes and adjacent regions 194, 123–138. https://doi.org/10.1016/S0031-0182(03)00274-8
- Ammann, C.M., Joos, F., Schimel, D.S., Otto-Bliesner, B.L., Tomas, R.A., 2007. Solar influence on climate during the past millennium: Results from transient simulations with the NCAR Climate System Model. Proc. Natl. Acad. Sci. 104, 3713–3718. https://doi.org/10.1073/pnas.0605064103
- Araguás-Araguás, L., Froehlich, K., Rozanski, K., 2000. Deuterium and oxygen-18 isotope composition of precipitation and atmospheric moisture. Hydrol. Process. 14, 1341–1355. https://doi.org/10.1002/1099-1085(20000615)14:8<1341::AID-HYP983>3.0.CO;2-Z
- Bowen, G.J., 2015. The online isotopes in precipitation calculator, version 2.2. http://www.waterisotopes.org.
- Bowen, G.J., Revenaugh, J., 2003. Interpolating the isotopic composition of modern meteoric precipitation: ISOTOPIC COMPOSITION OF MODERN PRECIPITATION. Water Resour. Res. 39. https://doi.org/10.1029/2003WR002086
- Bowen, G.J., Wassenaar, L.I., Hobson, K.A., 2005. Global application of stable hydrogen and oxygen isotopes to wildlife forensics. Oecologia 143, 337–348. https://doi.org/10.1007/s00442-004-1813-y
- Buso, D.C., Likens, G.E., 2007. Comparison of 15 evaporation methods applied to a small mountain lake in the northeastern USA. J. Hydrol. 340, 149–166. https://doi.org/10.1016/j.jhydrol.2007.03.018
- Cherkauer, D.S., Nader, D.C., 1989. Distribution of groundwater seepage to large surface-water bodies: The effect of hydraulic heterogeneities. J. Hydrol. 109, 151–165. https://doi.org/10.1016/0022-1694(89)90012-7

- Cherkauer, D.S., Zager, J.P., 1989. Groundwater interaction with a kettle-hole lake: Relation of observations to digital simulations. J. Hydrol. 109, 167–184. https://doi.org/10.1016/0022-1694(89)90013-9
- Cumming, B.F., Smol, J.P., 1993. Development of diatom-based salinity models for paleoclimatic research from lakes in British Columbia (Canada), in: van Dam, H. (Ed.), Twelfth International Diatom Symposium, Developments in Hydrobiology. Springer Netherlands, pp. 179–196.
- Dai, A., 2013. Increasing drought under global warming in observations and models. Nat. Clim. Change 3, 52–58. https://doi.org/10.1038/nclimate1633
- Dee, S.G., Parsons, L.A., Loope, G.R., Overpeck, J.T., Ault, T.R., Emile-Geay, J., 2017. Improved spectral comparisons of paleoclimate models and observations via proxy system modeling: Implications for multi-decadal variability. Earth Planet. Sci. Lett. 476, 34–46. https://doi.org/10.1016/j.epsl.2017.07.036
- Dee, S.G., Russell, J.M., Morrill, C., Chen, Z., Neary, A., 2018. PRYSM v2.0: A Proxy System Model for Lacustrine Archives. Paleoceanogr. Paleoclimatology 33, 1250–1269. https://doi.org/10.1029/2018PA003413
- Dee, S.G., Steiger, N.J., Emile-Geay, J., Hakim, G.J., 2016. On the utility of proxy system models for estimating climate states over the common era: DATA ASSIMILATION AND PROXY SYSTEM MODELS. J. Adv. Model. Earth Syst. 8, 1164–1179. https://doi.org/10.1002/2016MS000677
- Dinçer, T., 1968. The Use of Oxygen 18 and Deuterium Concentrations in the Water Balance of Lakes. Water Resour. Res. 4, 1289–1306. https://doi.org/10.1029/WR004i006p01289
- Edwards, T.W.D., Wolfe, B.B., Gibson, J.J., Hammarlund, D., 2004. Use of water isotope tracers in high latitude hydrology and paleohydrology, in: Smol, J.P., Pienitz, R., Douglas, M.S.V. (Eds.), Long-Term Environmental Change in Arctic and Antarctic Lakes, Developments in Paleoenvironmental Research. Springer Netherlands, Dordrecht, pp. 187–207. https://doi.org/10.1007/978-1-4020-2126-8_7
- Evans, M.N., Tolwinski-Ward, S.E., Thompson, D.M., Anchukaitis, K.J., 2013. Applications of proxy system modeling in high resolution paleoclimatology. Quat. Sci. Rev. 76, 16–28. https://doi.org/10.1016/j.quascirev.2013.05.024
- Gat, J.R., 1996. OXYGEN AND HYDROGEN ISOTOPES IN THE HYDROLOGIC CYCLE 39.
- Genereux, D., Bandopadhyay, I., 2001. Numerical investigation of lake bed seepage patterns: effects of porous medium and lake properties. J. Hydrol. 241, 286–303. https://doi.org/10.1016/S0022-1694(00)00380-2
- Gibson, J.J., 2002. A New Conceptual Model for Predicting Isotopic Enrichment of Lakes in Seasonal Climates. PAGES News 10, 10–11. https://doi.org/10.22498/pages.10.2.10
- Gibson, J.J., Birks, S.J., Yi, Y., 2016. Stable isotope mass balance of lakes: a contemporary perspective. Quat. Sci. Rev. 131, 316–328. https://doi.org/10.1016/j.quascirev.2015.04.013

- Gonfiantini, R., 1986. Environmental isotopes in lake studies. Handb. Environ. Isot. Geochem. Terr. Environ. 2, 113–168.
- Grosjean, M., Cartajena, I., Geyh, M.A., Nuñez, L., 2003. From proxy data to paleoclimate interpretation: the mid-Holocene paradox of the Atacama Desert, northern Chile. Palaeogeogr. Palaeoclimatol. Palaeoecol., Late-quaternary palaeoclimates of the southern tropical Andes and adjacent regions 194, 247–258. https://doi.org/10.1016/S0031-0182(03)00280-3
- Halder, J., Terzer, S., Wassenaar, L.I., Araguás-Araguás, L.J., Aggarwal, P.K., 2015. The Global Network of Isotopes in Rivers (GNIR): integration of water isotopes in watershed observation and riverine research. Hydrol. Earth Syst. Sci. 19, 3419–3431. https://doi.org/10.5194/hess-19-3419-2015
- Hargreaves, J.C., Annan, J.D., 2009. On the importance of paleoclimate modelling for improving predictions of future climate change. Clim. Past 5, 803–814. https://doi.org/10.5194/cp-5-803-2009
- Henderson, A.K., Shuman, B.N., 2009. Hydrogen and oxygen isotopic compositions of lake water in the western United States. GSA Bull. 121, 1179–1189. https://doi.org/10.1130/B26441.1
- Holmes, J.A., Zhang, J., Chen, F., Qiang, M., 2007. Paleoclimatic implications of an 850-year oxygen-isotope record from the northern Tibetan Plateau. Geophys. Res. Lett. 34. https://doi.org/10.1029/2007GL032228
- Horita, J., Wesolowski, D.J., 1994. Liquid-vapor fractionation of oxygen and hydrogen isotopes of water from the freezing to the critical temperature. Geochim. Cosmochim. Acta 58, 3425–3437. https://doi.org/10.1016/0016-7037(94)90096-5
- Hostetler, S.W., Benson, L.V., 1994. Stable isotopes of oxygen and hydrogen in the Truckee River-Pyramid Lake surface-water system. 2. A predictive model of δ^{18}O and 18^{2}H in Pyramid Lake. Limnol. Oceanogr. 39, 356–364. https://doi.org/10.4319/lo.1994.39.2.0356
- Johnson, T.C., Werne, J.P., Brown, E.T., Abbott, A., Berke, M., Steinman, B.A., Halbur, J., Contreras, S., Grosshuesch, S., Deino, A., Scholz, C.A., Lyons, R.P., Schouten, S., Damsté, J.S.S., 2016. A progressively wetter climate in southern East Africa over the past 1.3 million years. Nature 537, 220.
- Jones, M.D., Imbers, J., 2010. Modeling Mediterranean lake isotope variability. Glob. Planet. Change 71, 193–200. https://doi.org/10.1016/j.gloplacha.2009.10.001
- Jones, M.D., Leng, M.J., Roberts, C.N., Türkeş, M., Moyeed, R., 2005. A Coupled Calibration and Modelling Approach to the Understanding of Dry-Land Lake Oxygen Isotope Records. J. Paleolimnol. 34, 391–411. https://doi.org/10.1007/s10933-005-6743-0
- Kelts, K., Hsü, K.J., 1978. Freshwater Carbonate Sedimentation, in: Lerman, A. (Ed.), Lakes: Chemistry, Geology, Physics. Springer, New York, NY, pp. 295–323. https://doi.org/10.1007/978-1-4757-1152-3_9

- Kidmose, J., Nilsson, B., Engesgaard, P., Frandsen, M., Karan, S., Landkildehus, F., Søndergaard, M., Jeppesen, E., 2013. Focused groundwater discharge of phosphorus to a eutrophic seepage lake (Lake Væng, Denmark): implications for lake ecological state and restoration. Hydrogeol. J. 21, 1787–1802. https://doi.org/10.1007/s10040-013-1043-7
- Kim, S.-T., O'Neil, J.R., 1997. Equilibrium and nonequilibrium oxygen isotope effects in synthetic carbonates. Geochim. Cosmochim. Acta 61, 3461–3475. https://doi.org/10.1016/S0016-7037(97)00169-5
- Kim, S.-T., O'Neil, J.R., Hillaire-Marcel, C., Mucci, A., 2007. Oxygen isotope fractionation between synthetic aragonite and water: Influence of temperature and Mg2+ concentration. Geochim. Cosmochim. Acta 71, 4704–4715. https://doi.org/10.1016/j.gca.2007.04.019
- Kirby, M.E., Feakins, S.J., Bonuso, N., Fantozzi, J.M., Hiner, C.A., 2013. Latest Pleistocene to Holocene hydroclimates from Lake Elsinore, California. Quat. Sci. Rev. 76, 1–15. https://doi.org/10.1016/j.quascirev.2013.05.023
- Koschel, R.H., 1997. Structure and function of pelagic calcite precipitation in lake ecosystems. SIL Proc. 1922-2010 26, 343–349. https://doi.org/10.1080/03680770.1995.11900731
- Kumambala, P.G., Ervine, A., 2010. Water Balance Model of Lake Malawi and its Sensitivity to Climate Change. Open Hydrol. J. 4, 152–162. https://doi.org/10.2174/1874378101004010152
- Lempert, R.J., Groves, D.G., 2010. Identifying and evaluating robust adaptive policy responses to climate change for water management agencies in the American west. Technol. Forecast. Soc. Change 77, 960–974. https://doi.org/10.1016/j.techfore.2010.04.007
- Li, H.-C., Ku, T., 1997. δ13C-δ18O covariance as a paleohydrological indicator for closed-basin lakes. Palaeogeogr. Palaeoclimatol. Palaeoecol. 133, 69–80. https://doi.org/10.1016/S0031-0182(96)00153-8
- Lloyd, R.M., 1966. Oxygen isotope enrichment of sea water by evaporation. Geochim. Cosmochim. Acta 30, 801–814. https://doi.org/10.1016/0016-7037(66)90133-5
- Mann, M.E., Steinman, B.A., Miller, S.K., 2020. Absence of internal multidecadal and interdecadal oscillations in climate model simulations. Nat. Commun. 11, 49. https://doi.org/10.1038/s41467-019-13823-w
- Mann, M.E., Zhang, Z., Hughes, M.K., Bradley, R.S., Miller, S.K., Rutherford, S., Ni, F., 2008. Proxy-based reconstructions of hemispheric and global surface temperature variations over the past two millennia. Proc. Natl. Acad. Sci. 105, 13252–13257. https://doi.org/10.1073/pnas.0805721105
- Mark, S.Z., 2021. Amplified climatic variability and biomass burning are related on multiple timescales in the interior Pacific Northwest [Unpublished Manuscript]. Department of Geology and Environmental Science. University of Pittsburgh

- Mbanguka, R.P., Lyon, S.W., Holmgren, K., Girons Lopez, M., Jarsjö, J., 2016. Water Balance and Level Change of Lake Babati, Tanzania: Sensitivity to Hydroclimatic Forcings. Water 8, 572. https://doi.org/10.3390/w8120572
- Merlivat, L., Jouzel, J., 1979. Global climatic interpretation of the deuterium-oxygen 18 relationship for precipitation. J. Geophys. Res. 84, 5029. https://doi.org/10.1029/JC084iC08p05029
- Michelutti, N., Wolfe, A.P., Briner, J.P., Miller, G.H., 2007. Climatically controlled chemical and biological development in Arctic lakes: ARCTIC LAKE ONTOGENY. J. Geophys. Res. Biogeosciences 112, n/a-n/a. https://doi.org/10.1029/2006JG000396
- Morrill, C., Meador, E., Livneh, B., Liefert, D.T., Shuman, B.N., 2019. Quantitative model-data comparison of mid-Holocene lake-level change in the central Rocky Mountains. Clim. Dyn. 53, 1077–1094. https://doi.org/10.1007/s00382-019-04633-3
- Mote, P.W., Salathé, E.P., 2010. Future climate in the Pacific Northwest. Clim. Change 102, 29–50. https://doi.org/10.1007/s10584-010-9848-z
- Nelson, D.B., Abbott, M.B., Steinman, B.A., Polissar, P.J., Stansell, N.D., Ortiz, J.D., Rosenmeier, M.F., Finney, B.P., Riedel, J., 2011. A 6,000 year lake record of drought from the Pacific Northwest. Proc Natl Acad Sci USA 108, 3870–3875.
- Neukom, R., Gergis, J., Karoly, D.J., Wanner, H., Curran, M., Elbert, J., González-Rouco, F., Linsley, B.K., Moy, A.D., Mundo, I., Raible, C.C., Steig, E.J., van Ommen, T., Vance, T., Villalba, R., Zinke, J., Frank, D., 2014. Inter-hemispheric temperature variability over the past millennium. Nat. Clim. Change 4, 362–367. https://doi.org/10.1038/nclimate2174
- Otto-Bliesner, B.L., Russell, J.M., Clark, P.U., Liu, Z., Overpeck, J.T., Konecky, B., deMenocal, P., Nicholson, S.E., He, F., Lu, Z., 2014. Coherent changes of southeastern equatorial and northern African rainfall during the last deglaciation. Science 346, 1223–1227. https://doi.org/10.1126/science.1259531
- PAGES2k Consortium, 2017. A global multiproxy database for temperature reconstructions of the Common Era. Sci. Data 4, 170088. https://doi.org/10.1038/sdata.2017.88
- Palmer, W.C., 1965. Meteorological Drought. U.S. Department of Commerce, Weather Bureau.
- Pfannkuch, H.O., Winter, T.C., 1984. Effect of anisotropy and groundwater system geometry on seepage through lakebeds: 1. Analog and dimensional analysis. J. Hydrol. 75, 213–237. https://doi.org/10.1016/0022-1694(84)90051-9
- Rautio, A., Korkka-Niemi, K., 2011. Characterization of groundwater–lake water interactions at Pyhäjärvi, a lake in SW Finland 16, 18.
- Rinehart, C.D., Fox, K.F., 1976. Bedrock Geology of the Conconully Quadrangle, Okanogan County, Washington. U.S. Government Printing Office.
- Rosenberry, D.O., Lewandowski, J., Meinikmann, K., Nützmann, G., 2015. Groundwater - the disregarded component in lake water and nutrient budgets. Part 1: effects of groundwater on hydrology: EFFECTS OF GROUNDWATER ON

LAKE HYDROLOGY. Hydrol. Process. 29, 2895–2921. https://doi.org/10.1002/hyp.10403

- Rosenmeier, M.F., Brenner, M., Hodell, D.A., Martin, J.B., Curtis, J.H., Binford, M.W., 2016. A model of the 4000-year paleohydrology (δ18O) record from Lake Salpetén, Guatemala. Glob. Planet. Change, Climate Change and Archaeology in Mesoamerica: A Mirror for the Anthropocene 138, 43–55. https://doi.org/10.1016/j.gloplacha.2015.07.006
- Rozanski, K., Araguas-Araguas, L., Gonfiantini, R., 1992. Relation Between Long-Term Trends of Oxygen-18 Isotope Composition of Precipitation and Climate. Science 258, 981–985. https://doi.org/10.1126/science.258.5084.981
- Schewe, J., Heinke, J., Gerten, D., Haddeland, I., Arnell, N.W., Clark, D.B., Dankers, R., Eisner, S., Fekete, B.M., Colón-González, F.J., Gosling, S.N., Kim, H., Liu, X., Masaki, Y., Portmann, F.T., Satoh, Y., Stacke, T., Tang, Q., Wada, Y., Wisser, D., Albrecht, T., Frieler, K., Piontek, F., Warszawski, L., Kabat, P., 2014. Multimodel assessment of water scarcity under climate change. Proc. Natl. Acad. Sci. 111, 3245–3250. https://doi.org/10.1073/pnas.1222460110
- Schneider, R.L., Negley, T.L., Wafer, C., 2005. Factors influencing groundwater seepage in a large, mesotrophic lake in New York. J. Hydrol. 310, 1–16. https://doi.org/10.1016/j.jhydrol.2004.09.020
- Seal, R.R., Shanks, W.C., 1998. Oxygen and hydrogen isotope systematics of Lake Baikal, Siberia: Implications for paleoclimate studies. Limnol. Oceanogr. 43, 1251–1261. https://doi.org/10.4319/lo.1998.43.6.1251
- Shanahan, T.M., Overpeck, J.T., Sharp, W.E., Scholz, C.A., Arko, J.A., 2007. Simulating the response of a closed-basin lake to recent climate changes in tropical West Africa (Lake Bosumtwi, Ghana). Hydrol. Process. 21, 1678–1691. https://doi.org/10.1002/hyp.6359
- Shapley, M.D., Ito, E., Donovan, J.J., 2008. Isotopic evolution and climate paleorecords: modeling boundary effects in groundwater-dominated lakes. J. Paleolimnol. 39, 17–33. https://doi.org/10.1007/s10933-007-9092-3
- Shaw, R.D., Prepas, E.E., 1990. Groundwater-lake interactions: I. Accuracy of seepage meter estimates of lake seepage. J. Hydrol. 119, 105–120. https://doi.org/10.1016/0022-1694(90)90037-X
- Shuman, B., Pribyl, P., Minckley, T.A., Shinker, J.J., 2010. Rapid hydrologic shifts and prolonged droughts in Rocky Mountain headwaters during the Holocene. Geophys. Res. Lett. 37. https://doi.org/10.1029/2009GL042196
- Solotchina, E.P., Sklyarov, E.V., Solotchin, P.A., Vologina, E.G., Sklyarova, O.A., 2014. Mineralogy and crystal chemistry of carbonates from the Holocene sediments of Lake Kiran (western Transbaikalia): connection with paleoclimate. Russ. Geol. Geophys. 55, 472–482. https://doi.org/10.1016/j.rgg.2014.03.005
- Stansell, N.D., Steinman, B.A., Abbott, M.B., Rubinov, M., Roman-Lacayo, M., 2013. Lacustrine stable isotope record of precipitation changes in Nicaragua during the Little Ice Age and Medieval Climate Anomaly. Geology 41, 151–154. https://doi.org/10.1130/G33736.1

- Stansell, N.D., Steinman, B.A., Lachniet, M.S., Feller, J., Harvey, W., Fernandez, A., Shea, C.J., Price, B., Coenen, J., Boes, M., Perdziola, S., 2020. A lake sediment stable isotope record of late-middle to late Holocene hydroclimate variability in the western Guatemala highlands. Earth Planet. Sci. Lett. 542, 116327. https://doi.org/10.1016/j.epsl.2020.116327
- Steinman, B.A., Abbott, M.B., Mann, M.E., Stansell, N.D., Finney, B.P., 2012. 1,500 year quantitative reconstruction of winter precipitation in the Pacific Northwest. Proc. Natl. Acad. Sci. 109, 11619–11623. https://doi.org/10.1073/pnas.1201083109
- Steinman, B.A., Abbott, M.B., Nelson, D.B., Stansell, N.D., Finney, B.P., Bain, D.J., Rosenmeier, M.F., 2013. Isotopic and hydrologic responses of small, closed lakes to climate variability: Comparison of measured and modeled lake level and sediment core oxygen isotope records. Geochim. Cosmochim. Acta 105, 455–471. https://doi.org/10.1016/j.gca.2012.11.026
- Steinman, B.A., Mann, M.E., Miller, S.K., 2015. Atlantic and Pacific multidecadal oscillations and Northern Hemisphere temperatures. Science 347, 988–991. https://doi.org/10.1126/science.1257856
- Steinman, B.A., Nelson, D.B., Abbott, M.B., Stansell, N.D., Finkenbinder, M.S., Finney, B.P., 2019. Lake sediment records of Holocene hydroclimate and impacts of the Mount Mazama eruption, north-central Washington, USA. Quat. Sci. Rev. 204, 17–36. https://doi.org/10.1016/j.quascirev.2018.09.018
- Steinman, B.A., Rosenmeier, M.F., Abbott, M.B., 2010a. The isotopic and hydrologic response of small, closed-basin lakes to climate forcing from predictive models: Simulations of stochastic and mean state precipitation variations. Limnol. Oceanogr. 55, 2246–2261. https://doi.org/10.4319/lo.2010.55.6.2246
- Steinman, B.A., Rosenmeier, M.F., Abbott, M.B., 2010b. The isotopic and hydrologic response of small, closed-basin lakes to climate forcing from predictive models: Simulations of stochastic and mean state precipitation variations. Limnol. Oceanogr. 55, 2246–2261. https://doi.org/10.4319/lo.2010.55.6.2246
- Tierney, J.E., Smerdon, J.E., Anchukaitis, K.J., Seager, R., 2013. Multidecadal variability in East African hydroclimate controlled by the Indian Ocean. Nature 493, 389–392. https://doi.org/10.1038/nature11785
- Vainu, M., Terasmaa, J., Häelm, M., 2015. Relations between groundwater flow in an unconfined aquifer and seepage patterns in a closed-basin lake in glacial terrain. Hydrol. Res. 46, 325–342. https://doi.org/10.2166/nh.2014.197
- Valiantzas, J.D., 2006. Simplified versions for the Penman evaporation equation using routine weather data. J. Hydrol. 331, 690–702. https://doi.org/10.1016/j.jhydrol.2006.06.012
- Vassiljev, J., Harrison, S.P., Haxeltine, A., 1995. Recent lake-level and outflow variations at Lake Viljandi, Estonia: validation of a coupled lake-catchment

modelling scheme for climate change studies. J. Hydrol. 170, 63–77. https://doi.org/10.1016/0022-1694(95)02691-H

- Vogt, H.J., 1976. Isotopentrennung bei der Verdunstung von Wasser. Staatsexamensarbeit Inst. Für Umweltphysik Heidelb. Ger.
- Vorosmarty, C.J., 2000. Global Water Resources: Vulnerability from Climate Change and Population Growth. Science 289, 284–288. https://doi.org/10.1126/science.289.5477.284
- Williams, D.F., 1997. Lake Baikal Record of Continental Climate Response to Orbital Insolation During the Past 5 Million Years. Science 278, 1114–1117. https://doi.org/10.1126/science.278.5340.1114
- Wise, E.K., Dannenberg, M.P., 2017. Reconstructed storm tracks reveal three centuries of changing moisture delivery to North America. Sci. Adv. 3, e1602263. https://doi.org/10.1126/sciadv.1602263
- Yao, H., Scott, L., Guay, C., Dillon, P., 2009. Hydrological impacts of climate change predicted for an inland lake catchment in Ontario by using monthly water balance analyses. Hydrol. Process. 23, 2368–2382. https://doi.org/10.1002/hyp.7347
- Yu, Z., 2000. Ecosystem response to Lateglacial and early Holocene climate oscillations in the Great Lakes region of North America. Quat. Sci. Rev. 19, 1723–1747. https://doi.org/10.1016/S0277-3791(00)00080-9